Multi-site disease analytics with applications to estimating COVID-19 undetected cases in Canada

Matthew R. P. Parker[1,‡],   Jiguo Cao[1,†],   Laura L. E. Cowen[2,†,‡],
Lloyd T. Elliott[1,†],   Junling Ma[2,†]

[1]Department of Statistics and Actuarial Science, Simon Fraser University, Canada
[2]Department of Mathematics and Statistics, University of Victoria, Canada

July 2022

Abstract

Even with daily case counts, the true scope of the COVID-19 pandemic in Canada is unknown due to undetected cases. We estimate the pandemic scope through a new multi-site model using publicly available disease count data including detected cases, recoveries among detected cases, and total deaths. These counts are used to estimate the case detection probability, the infection fatality rate through time, as well as the probability of recovery, and several important population parameters including the rate of spread, and importation of external cases. We also estimate the total number of active COVID-19 cases per region of Canada for each reporting interval. We applied this multi-site model Canada-wide to all provinces and territories, providing an estimate of the total COVID-19 burden for the 90 weeks from 23 Apr 2020 to 6 Jan 2022. We also applied this model to the five Health Authority regions of British Columbia, Canada, describing the pandemic in B.C. over the 31 weeks from 2 Apr 2020 to 30 Oct 2020.

1 Introduction

The novel coronavirus pandemic began in December 2019, and spread rapidly to every corner of the globe. The impact of the pandemic on lives, societal and social norms, and on the world economy cannot be overstated (Béland et al., 2021; Cypress, 2022; Tanaka, 2022). As of late June 2022, the global total number of deaths attributed to the pandemic is over 6.3 million, from a recorded total of 540 million reported cases. And Canada has recorded a total of over 3.9 million confirmed cases, and over 41 thousand confirmed deaths (Dong et al., 2020). The number of confirmed cases of coronavirus are an under-reporting of the true total (see for example: Feikin et al., 2020; Buitrago-Garcia et al., 2020; Hasan et al., 2021; Chisale et al., 2022). The reasons for under-reporting are varied and include the presence of asymptomatic, pauci-symptomatic, and pre-symptomatic cases, lack of testing for low severity cases, and periods with low testing volumes. Some of these causes can be controlled through testing protocols and wider availability/accessibility of testing. However, due to the impracticality of full census testing of large populations in Canada, under-reporting cannot

---

† Authors listed in alphabetical order.

‡ Address correspondence to Matthew R. P. Parker *(matthew_parker_2@sfu.ca)* and Dr. Laura L. E. Cowen *(lcowen@uvic.ca)*.

be entirely mitigated. Undetected cases cause community infections, and reduces the effectiveness of control measures such as contact tracing, quarantine and isolation. They also cause underestimates of the social and economical impacts of the pandemic.

To properly understand the scope and impact of the pandemic, we must estimate the true total number of infections. Research conducted after the pandemic began has improved methodologies to produce such estimates. These methods include meta-analyses of asymptomatic prevalence (He et al., 2021; Alene et al., 2021), extensions to susceptible-infectious-recovered type modelling (Li et al., 2021; Subramanian et al., 2021; Huo et al., 2021), and seroprevalence studies (Bendavid et al., 2021; Saeed et al., 2021; Halili et al., 2022). Alternative models include integer-autoregressive models (Fernández-Fontelo et al., 2020) and case fatality rate (CFR) models (Dougherty et al., 2021), and estimating under-reporting using discrete count models (Parker et al., 2021).

Much research has focused on understanding the course of the pandemic within Canada. Examples include seroprevalence of Montréal school age children (Zinszer et al., 2021), CFR based models to estimate reporting rates across Canada (Dougherty et al., 2021), intervention strategy analysis in Ontario (Tuite et al., 2020), mental health and well-being of Canadians during the pandemic (Dozois, 2021; Appleby et al., 2022), models to forecast transmission and incidence (Chimmula and Zhang, 2020; Mullah and Yan, 2022), and policy response analysis with comparisons between Canada, France, and Belgium (Desson et al., 2020). Among this backdrop of vital research, we provide up-to-date disease analytics for Canada as a whole, with results specific to each province and territory.

We propose a novel multi-site modelling technique to better estimate disease dynamics such as domestic spread rate, recovery and death probabilities, and to estimate effectiveness of testing protocols and levels of under-reporting of cases. By considering data from across the entire time span of the pandemic, estimates can be made throughout its course. Multi-site modelling allows the total burden of the pandemic to be estimated across large regions by considering them as an amalgamation of smaller regions. This method of modelling increases precision compared to single site modelling, by pooling information across sites, which is an example of transfer learning (Weiss et al., 2016). To analyze the burden of COVID-19 as it has progressed through time in Canada, we model the entire pandemic period to date (from 23 Apr 2020 to 6 Jan 2022).

Our multi-site hidden Markov model has several new mathematical contributions in comparison with the single-site model (Parker et al., 2021): We provide a multi-site framework for disease analytics, we add a saturation effect to model limitations on disease spread, and we model the disease spread rate separately for the detected and the undetected disease cases. The latent states in our model are identifiable due to parametric assumptions. This is similar to the modelling of population abundance in open population N-mixtures models (Dail and Madsen, 2011).

We investigate the effect of vaccination coverage on virus spread rates, recovery probability, and death probability through inclusion of a vaccine coverage covariate. We also include indicators for time periods demarcated by the first confirmed cases in Canada of the variants of concern Delta (Mahumud et al., 2022) and Omicron (Araf et al., 2022), which have been shown to have very different vaccine efficacies (Kahn et al., 2022). These indicators allow us to model changes in disease dynamics and interaction between vaccine efficacy and the dominant variant of concern.

The main contributions of this paper are (1) a novel multi-site disease analytics model, (2) estimates of the
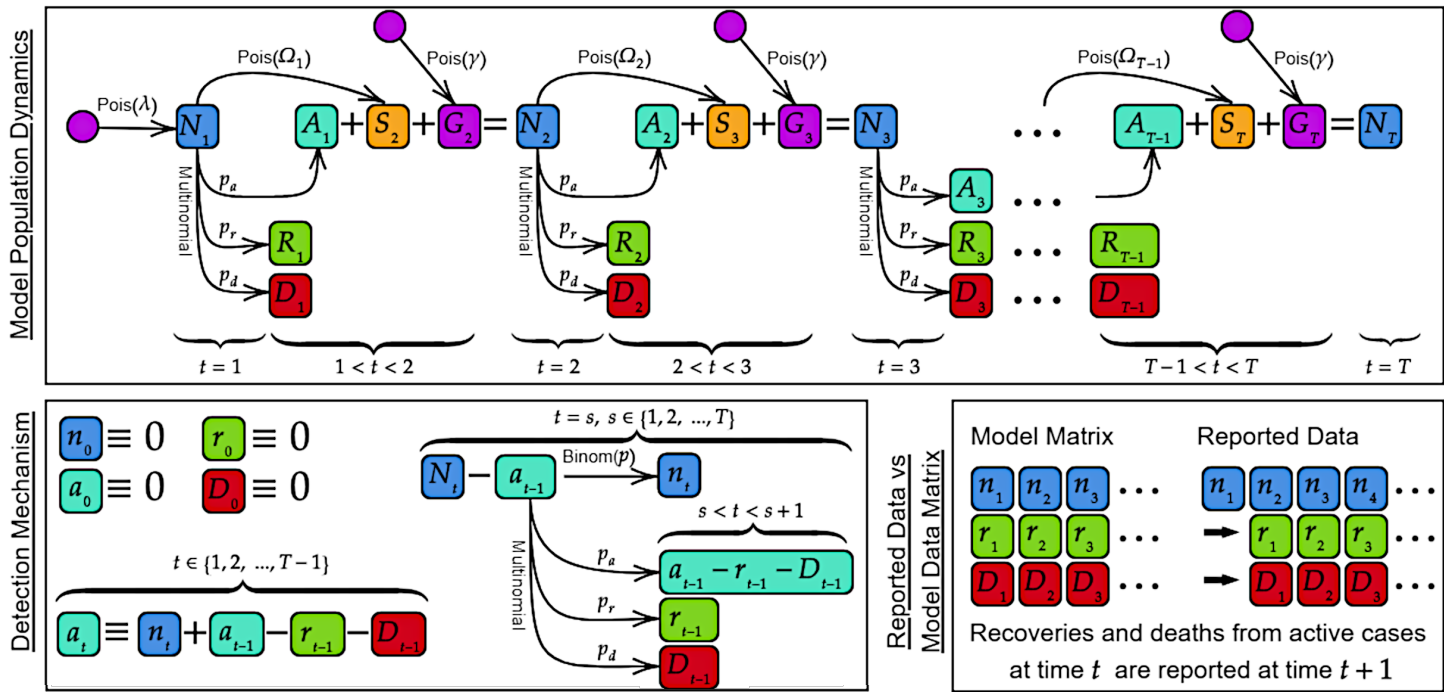
Figure 1: Diagram of single-site model. Top: The disease dynamics and state process. Bottom left: The detection mechanisms. Bottom right: Data reporting times.

total burden of COVID-19 across Canada for 90 weeks of the pandemic, (3) estimates of reporting rates for each province and territory of Canada, (4) estimates of domestic spread rates among both detected and undetected cases, (5) estimates of infection fatality rate (IFR) for COVID-19 in Canada, (6) estimates of average recovery period for active cases, and (7) comparisons between competing models.

2 Methods

2.1 Multi-site Model

In our new multiple-site disease analytics model, each site is treated as statistically independent, so that the likelihood function is a product of single-site likelihoods. Figure 1 outlines the single-site model including the disease dynamics (top panel), detection mechanisms (bottom left panel), and the difference between the model definition of the data and the actual reporting times (bottom right panel).

Let n_{it} denote the new detected case counts at sampling occasion $t = 1, \ldots, T$ and study site $i = 1, \ldots, M$. The new detected recoveries between t and $t + 1$ among all detected active cases are r_{it}. The new detected deaths between t and $t + 1$ are d_{it} (when deaths are fully detected, we let $d_{it} = D_{it}$, and D_{it} cease to be considered latent states). The total number of active cases at time t are N_{it}, and a_{it} cases among them are detected. The active cases at time t that will recover, die, or remain active between t and $t + 1$ are respectively R_{it}, D_{it}, A_{it}. In the following we split the model into ten components for ease of understanding:

3

(1)	Initial Abundance:	$N_{i1} \sim \text{Poisson}(\lambda)$
(2)	State Process:	$\{A_{it}, D_{it}, R_{it}\} \sim \text{Multinomial}(N_{it}; p_a, p_d, p_r)$
(3)	Detected Active Cases:	$a_{it} = n_{it} + a_{it-1} - r_{it-1} - d_{it-1}$, for $t > 0$
(4)	Domestic Spread:	$S_{it} \sim \text{Poisson}(\Omega_{it-1})$, for $t > 1$
(5)	Ω_{it-1} :	$\omega_1(N_{it-1} - a_{it-1}) \cdot \delta_i + \omega_2 a_{it-1}$ (mean domestic spread)
(6)	δ_i :	$(H_i - N_{it})/H_i$ (fraction of susceptible population. Here H_i is the total population size)
(7)	Imported Cases:	$G_{it} \sim \text{Poisson}(\gamma)$, for $t > 1$
(8)	Abundance Updates:	$N_{it} = A_{it-1} + S_{it} + G_{it}$, for $t > 1$
(9)	Observation Process I:	$n_{it} \sim \text{Binomial}(N_{it} - a_{it-1}, p)$
(10)	Observation Process II:	$\{a_{it} - d_{it} - r_{it}, d_{it}, r_{it}\} \sim \text{Multinomial}(a_{it}; p_a^*, \alpha p_d, p_r)$

Component (1) describes the initial abundance where λ is defined as the expected initial population size. The latent state process (Component 2) partitions each active case in N_{it} at time t into one of the three categories A_{it}, D_{it}, and R_{it}, with probabilities p_a, p_d, and p_r, according to whether each case will remain active, die, or recover by time $t + 1$. Here $p_a = 1 - p_r - p_d$. We assume that individuals are indistinguishable, which is a requirement for these aggregate data models, and leads to p_r and p_d being constant across individuals, and is a justification for the choice of using the multinomial distribution. Component (3) provides the calculation for a_{it} the number of detected cases still active at time t. The value of a_{it} is entirely specified by the observed data. We calculate a_{it} recursively, with a_{i0}, r_{i0}, d_{i0}, n_{i0} all zero by definition, except when detected active cases are known from the time period prior to $t = 1$, in which case a_{i0} would not be zero. In Component (4), S_{it} models the domestic spread rate, which is the spread of the disease due to contact with infectious individuals within the population during each time interval. We make the simplifying assumption that the transmission rate remains constant unless mediated by additional covariates, so that the Poisson distribution is a reasonable choice. S_{it} allows for exponential growth of cases, but does not allow a spontaneous outbreak within a population having zero active cases. Ω_{it} is the average new infections per time interval, which is calculated using the two parameters ω_1 and ω_2 (Component 5). The basic reproductive number R_0 is the product of Ω and the mean infectious period ($1/p_r$). Parameters ω_1 and ω_2 are the average new infections per undetected ($N_{it-1} - a_{it-1}$) and detected (a_{it-1}) active case, respectively. Component (6) describes the value δ_i that modulates the growth of cases as the population becomes saturated with infection. Here H_i is the total population size of site i, which is the maximum number of infected individuals that are possible in that region. δ_i decreases to zero linearly as N_{it} approaches H_i, implying that the spread rate goes to zero as the population becomes fully saturated. Imported cases, G_{it}, are new cases entering the population (Component 7), for example from travel. The parameter γ is the average new number of imported cases per time interval. Imported cases allow for disease to occur even when $N_{i1} = 0$, allowing for spontaneous outbreaks in regions with no previous active cases. G_{it} allows for linear growth of cases over time. The number of cases N_{it} changes with time (Component 8), so we calculate the abundance updates for $t > 1$ using A_{it} from the state process as well as the growth terms S_{it} and G_{it}, giving $N_{it} = A_{it-1} + S_{it} + G_{it}$. Component (9) describes the reporting of case counts where p is the probability of detecting a case, and so $1 - p$ gives the under-reporting rate. We would like to have $n_{it} \sim \text{Binomial}(N_{it}, p)$, which is the traditional N-mixtures parameterization of detection probability (Royle, 2004). However, since N_{it} comprises all active cases, including those which have already been detected, this would allow double counting (because detected cases n_{it} are tracked until recovery or death). Instead, we subtract the already detected active cases prior to the binomial thinning:

$N_{it} - a_{it-1}$. Individuals are indistinguishable for these aggregate count models, and so we choose the binomial distribution to model detection. Component (10) models the reporting of recoveries and deaths by partitioning a_{it} into cases that remain active, cases that die, and cases that recover. We use $\alpha = 1$ when deaths are under-reported. In the situation where deaths are considered to be fully reported (when detected deaths are D_{it} rather than d_{it}), we set $\alpha = 1/p$, which increases the proportion of deaths among detected cases compared to proportion of deaths among all cases. Note that $p_a^* = 1 - \alpha p_d - p_r$.

We have built on the Parker et al. (2021) model to allow for multiple sites, which in our B.C. case study corresponds to the five Health Authority Regions of B.C., and which in our Canada-wide case study corresponds to the provinces and territories of Canada. Deaths and recoveries are occasionally recorded directly during the first observation period for an individual (such as when a recovery or death occurs in the same week as the initial positive test result). This leads to a small simplification of the detection process: $n_{it} \sim \text{Binomial}(p, N_{it} - a_{it-1})$ rather than $n_{it} \sim \text{Binomial}(p, N_{it} - a_{it} + d_{it} + r_{it})$. With this improvement, we not only continue to avoid double counting cases, but also allow deaths and recoveries to occur in the same reporting period as the first observation for an individual. We have split the spread rate ω into two new parameters ω_1 and ω_2. This allows us to model different domestic spread rates due to detected and undetected cases. To account for local cluster saturation and population saturation effects, we incorporated a penalty term to the model which allows ω_1 to diminish as the number of active cases increases. By using the known population size of a region as an upper bound on total possible infections, we linearly reduce the domestic spread to zero when the population is saturated, replacing $\omega_1(N_{it} - a_{it})$ with $\omega_1(N_{it} - a_{it})(H_i - N_{it})/H_i$. Here H_i is the total population of region i. An exponential decay could be considered rather than linear decay if case cluster saturation is expected to be a dominant effect, which can be explored in future work. The penalty term has the additional benefit of penalizing "infinite abundances", which can be an issue for N-mixture type models (Dennis et al., 2015; Barker et al., 2018). The full joint distribution for our multi-site model is thus $f(\lambda, \gamma, \omega_1, \omega_2, p, p_r, p_d, \{n_{it}\}, \{r_{it}\}, \{d_{it}\}) = \mathscr{L} \cdot \pi_\lambda \cdot \pi_\gamma \cdot \pi_{\omega_1} \cdot \pi_{\omega_2} \cdot \pi_p \cdot \pi_{p_d} \cdot \pi_{p_r}$ with likelihood function $\mathscr{L}$ given by the following equation:

$$
\begin{aligned}
\mathscr{L} = \prod_{i=1}^{M} &\left(\text{Poisson}(N_{i1}; \lambda) \cdot \left(\prod_{t=1}^{T} \text{Binomial}(n_{it}; N_{it} - a_{it-1}, p) \cdot \text{Multinomial}(A_{it}, D_{it}, R_{it}; N_{it}, p_a, p_d, p_r) \right) \times \right. \\
&\left(\prod_{t=1}^{T-1} \text{Multinomial}(a_{it} - d_{it} - r_{it}, d_{it}, r_{it}; a_{it}, p_a, p_d, p_r) \right) \times \\
&\left. \left(\prod_{t=2}^{T} \text{Poisson}(G_{it}; \gamma) \cdot \text{Poisson}\left(S_{it}; \omega_1(N_{it-1} - a_{it-1}) \cdot (H_i - N_{it})/H_i + \omega_2 a_{it-1} \right) \right) \right).
\end{aligned}
$$

(1)

Here π_x is the prior distribution chosen for parameter x. Note that while the sites are independent conditioned on their parameters, the likelihood shares parameters across sites. Parameters can be separated across sites or pooled by grouping sites using categorical site covariates. A single-site model can be obtained by dropping the site subscript i from Equation 1 (Appendix S.1). We also conducted a simulation study to verify parameter identifiability for our multi-site model (Appendix S.2).

5

2.2   Model Fitting

We used Bayesian Markov-chain Monte-Carlo (MCMC) methods for parameter estimation and implemented model fitting using the statistical computing software R (R Core Team, 2022), together with the R package *Nimble* for probabilistic programming (de Valpine et al., 2017, 2021). We mainly used uninformative uniform prior distributions with reasonable upper and lower bounds. For example, ω_1 was given a prior of Uniform$(0, 5)$, as $\omega_1 \geq 0$, and an ω_1 of 5 is far larger than would be expected. Our investigations indicate that with the exception of extreme priors, parameter estimates were not sensitive to the prior. We found that a burn-in of 100,000 was usually enough for the MCMC chains to converge. However, for some combinations of data and covariates a burn-in of 1,000,000 was necessary. We used 200,000 iterations, which was more than sufficient to produce posterior estimates.

3   Applications

3.1   Case Study: Canada

3.1.1   Data Sources

We used three publicly available sources of data for our Canada case study. The majority of the data came from the Government of Canada's COVID-19 daily epidemiology update (PHAC: Government of Canada, 2022a), which contains testing volumes, case counts, recoveries, and deaths due to COVID-19 for each province and territory from 23 Apr 2020 to 6 Jan 2022. However, the testing volumes for the Yukon Territory were largely missing from 3 Jun 2021 onward. For this reason we used the testing volume data reported by Yukon Health (Government of Yukon, 2022) to supplement the PHAC data. Our third set of data was the provincial vaccination status reports, also from the PHAC (Government of Canada, 2022b). These reports include total counts per province of individuals who had received one vaccination shot, and who had received at least two vaccination shots. All count data were aggregated by week to alleviate the issue of lump sum data reporting (such as when COVID-19 cases detected over a weekend are only reported after the weekend). After aggregation, we were left with 90 weeks of data for model fitting.

3.1.2   Parameter Covariates

We chose several parameter covariates for the Canada-wide model. Both λ and γ were allowed to vary by site (province/territory). We used weekly testing volume as a covariate for detection probability, since more testing should lead to higher detection rates. Figure S10 in the Appendix shows the testing volume data for each site. Vaccination rates (at least one dose and two doses) were used as covariates for the parameters p_r, p_d, ω_1, ω_2, and γ. Figure S11 in the Appendix shows the vaccination rates as a portion of the total population. Single dose rates are shown in red, while second dose rates are shown in blue. The vaccination rates for the Northwest Territories indicate a data anomaly in June 2021, where both single and double dose rates were reduced. This may be due to a data correction which occurred in June 2021.

The dates of emergence in Canada for the two variants of concern—Delta and Omicron—were used as covariates for time period change points for the variables γ, ω_1, and ω_2. As start date for the time periods, we used the first week of confirmed cases in Canada, 4 Apr 2021 (week 51) for Delta, and 28 Nov 2021 (week 84) for Omicron.

3.1.3   Results

Figure 2 shows both the detected case counts n_{it} and the estimated total active cases $\widehat{N}_{it}$ for each site (province or territory). Due to the exponential growth and decay in case numbers, the active cases are plotted on a log scale. Every site saw a large increase in cases during the Omicron time period, whereas the Delta time period saw an initial drop in cases from May to August 2021 in most sites.

The detection probability $\widehat{p}$ changes over time due to testing volumes (Figure 3). Detection rates in Newfoundland and Labrador, Nunavut, and Yukon were much lower than other sites for the majority of the pandemic, while the Prince Edward Island detection rate was consistently higher than 35%. Several provinces (such as B.C., Ontario, and Quebec) showed consistent growth in detection rates over the course of the pandemic, with a shared noticeable slump during the first four months of the Delta time period.

The probability of death, $\widehat{p}_d$, was seen to hold steady at 0.26% in all sites for the first period of the pandemic, before decreasing (Figure S12 in the Appendix). The effect of vaccinations on p_d is seen as a dramatic decrease throughout early 2021. The Delta period saw an increase in p_d, which was ameliorated by increasing vaccination coverage in each site. The Omicron period saw a sharp drop in mortality, with p_d levelling out around 0.06% across Canada. Nunavut saw a larger probability of death during the Delta time period than the other sites, with a 95% credible interval of (0.19, 0.20)%, which does not overlap with any of the other site credible intervals. The three territories saw probability of death drop earlier than the provinces, likely due to earlier vaccination drives within the territories; Yukon reached 60% vaccination by 15 May 2021, while Saskatchewan reached 60% by 26 Jun 2021. The median death probabilities are shown in Table S1 in the Appendix.

Probability of recovery was steady at 35.0% during the early stages of the pandemic for all sites until January 2021 when the recovery probability began to increase along with the increase in vaccination coverage across Canada (Figure S13 in the Appendix). The Delta period saw a small decrease in recovery probability for all sites, while the Omicron period saw a large decrease. Probability of recovery peaked much earlier for the three territories than for any of the provinces, likely due to the earlier vaccination drives in the territories. The median recovery probabilities are shown in Table S2 in the Appendix.

The domestic spread for undetected cases, $\widehat{\omega}_1$, accounted for most cases in the pre-2021 period (Figure 4). As vaccination coverage increased across Canada, the spread rate for detected cases, $\widehat{\omega}_2$, increased, and in all sites became larger than the spread rate for undetected cases during the Delta time period. During the Omicron time period, the two spread rates converged to similar levels. During the early pandemic, Prince Edward Island had the largest spread rate among undetected cases, with a 95% credible interval of (1.11, 1.26), much larger than the Canada wide average of (0.55,0.59). During this early pandemic period, Yukon had the lowest rate, with a 95% credible interval of (0.25,0.36). Conversely, the spread rate among detected cases was much smaller, with the Canada wide average having a 95% credible interval of (0.14, 0.32). In the Omicron period, the spread rate for undetected cases was less than the spread rate for detected cases, with the Canada wide 95% credible intervals of (1.17,1.21) and (1.22,1.62) respectively. The median spread rates are shown in Table S3 for undetected, and in Table S4 for detected cases in the Appendix.

Weekly importation rates, $\widehat{\gamma}$, are generally low across Canada, with the exceptions of Quebec and British Columbia (Figure S14 in the Appendix). British Columbia had the second largest importation rate, at around 80 imported cases per week. Quebec had the largest, at around 1,400 imported cases per week. It is
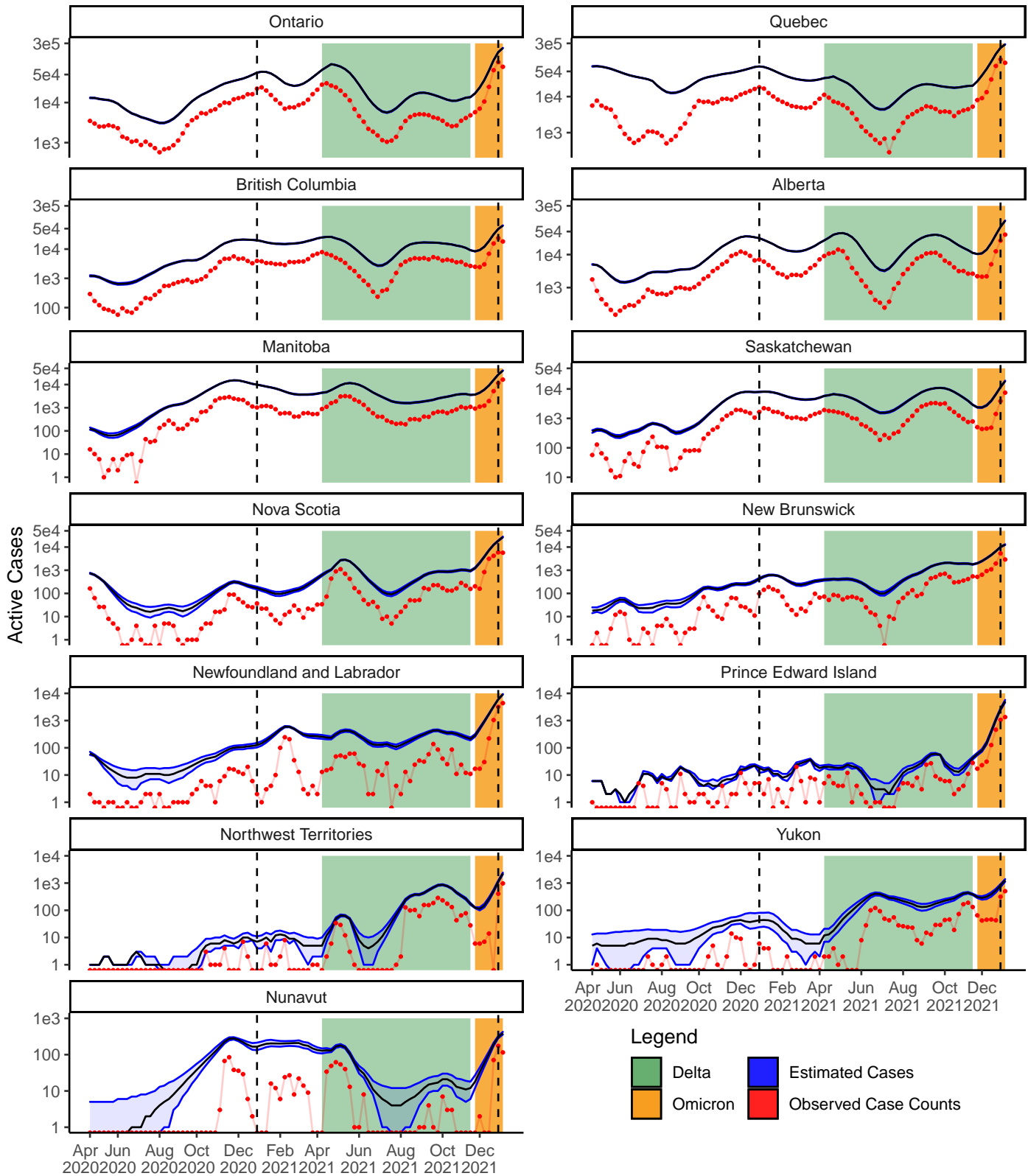
Figure 2: Detected case counts (red) and estimated total active cases (blue) for each province/territory from 23 Apr 2020 to 6 Jan 2022. The time periods for the two variants of concern Delta and Omicron are depicted with coloured bands. The two vertical dashed lines indicate 1 Jan 2021 and 1 Jan 2022. Active cases are plotted on a log scale. Bands indicate 95% credible intervals.
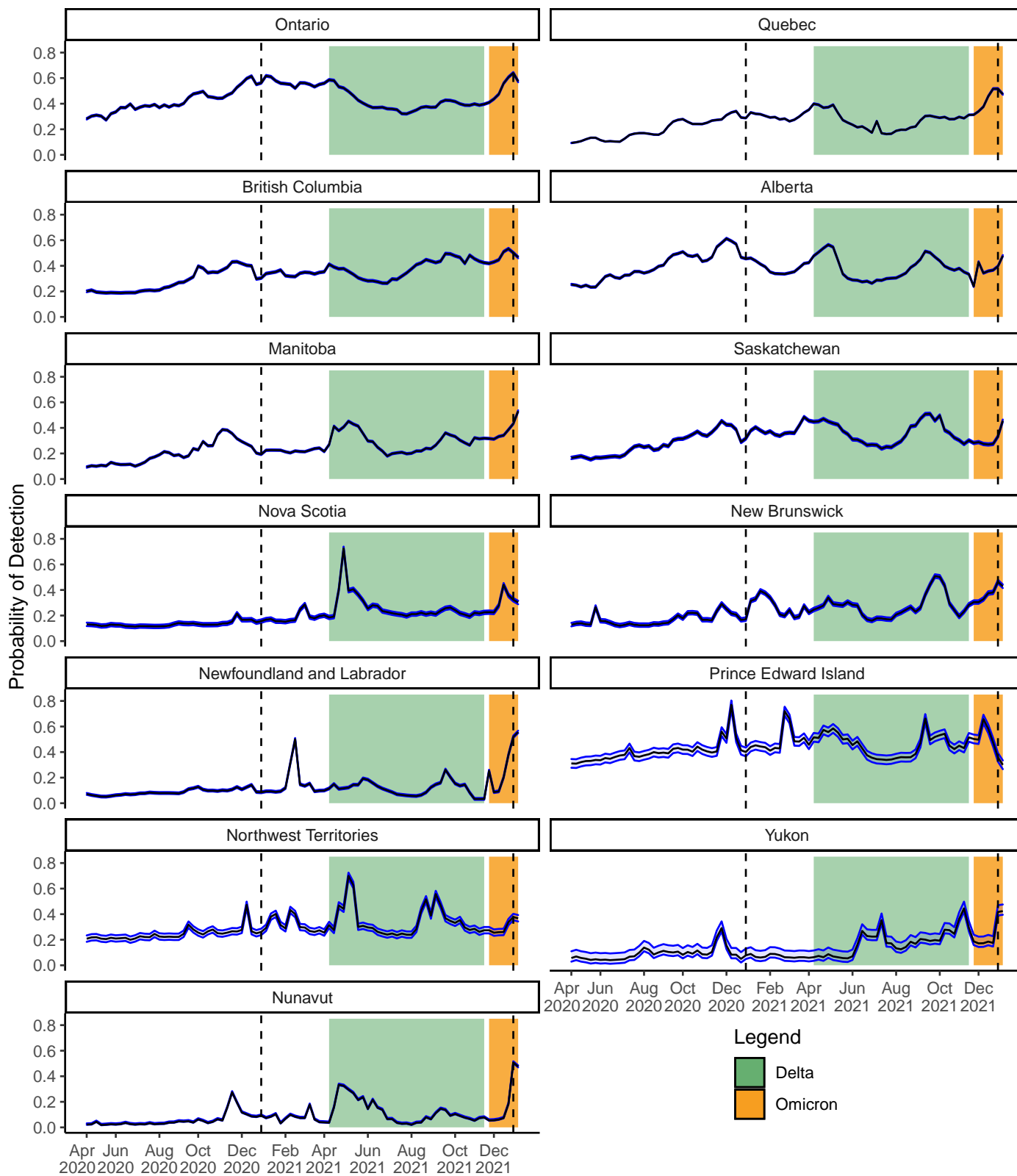
Figure 3: Estimated weekly detection probability (blue) for active COVID-19 cases for each province or territory from 23 Apr 2020 to 6 Jan 2022. The time periods for the two variants of concern—Delta and Omicron—are depicted with coloured bands. The two vertical dashed lines indicate 1 Jan 2021 and 1 Jan 2022. Bands show 95% credible intervals.
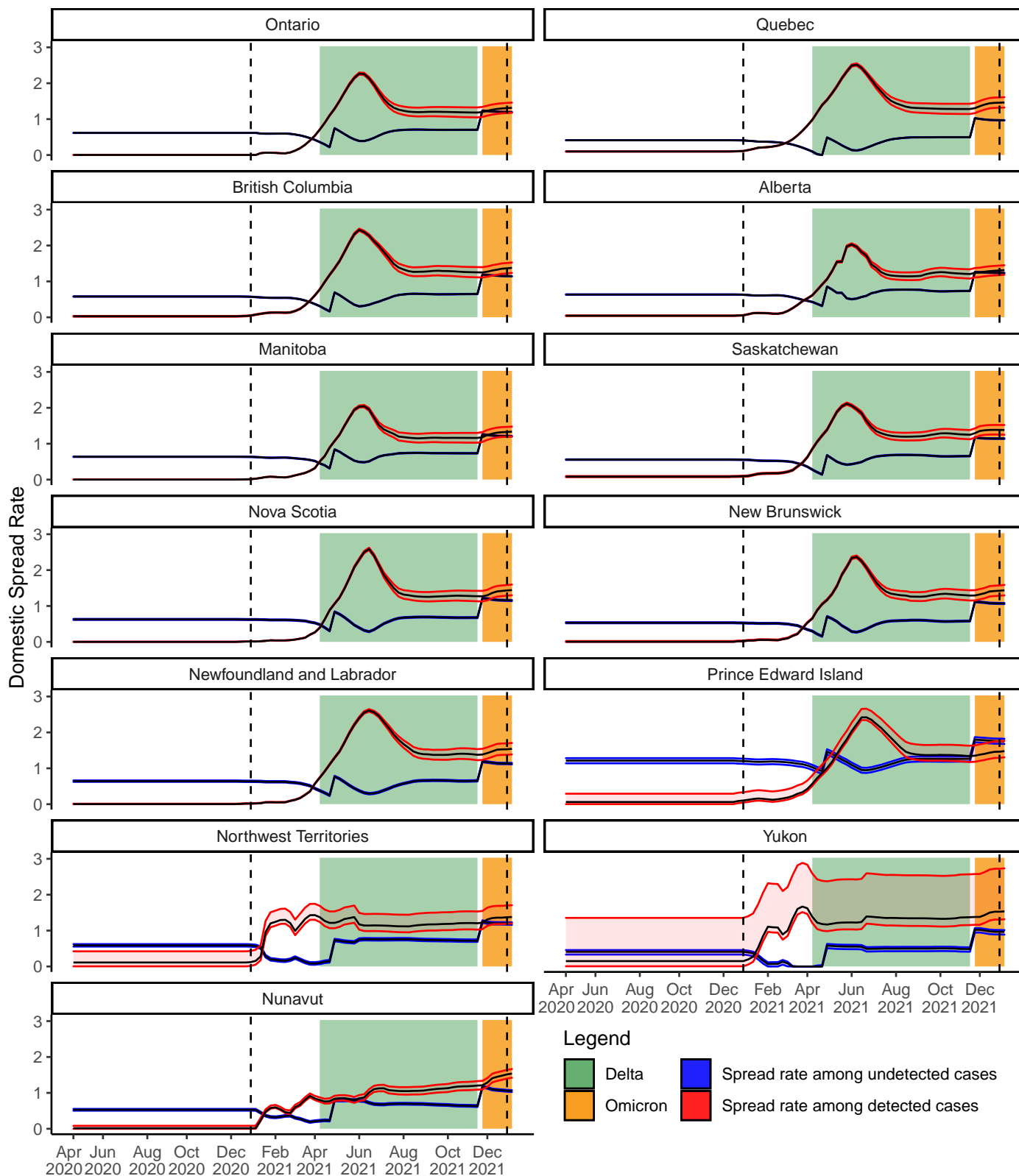
Figure 4: Estimated weekly domestic spread rates for detected (red, $\widehat{\omega}_2$) and undetected (blue, $\widehat{\omega}_1$) active COVID-19 cases for each province/territory from 23 Apr 2020 to 6 Jan 2022. The time periods for the two variants of concern Delta and Omicron are depicted with coloured bands. The two vertical dashed lines indicate 1 Jan 2021 and 1 Jan 2022. Bands show 95% credible intervals.
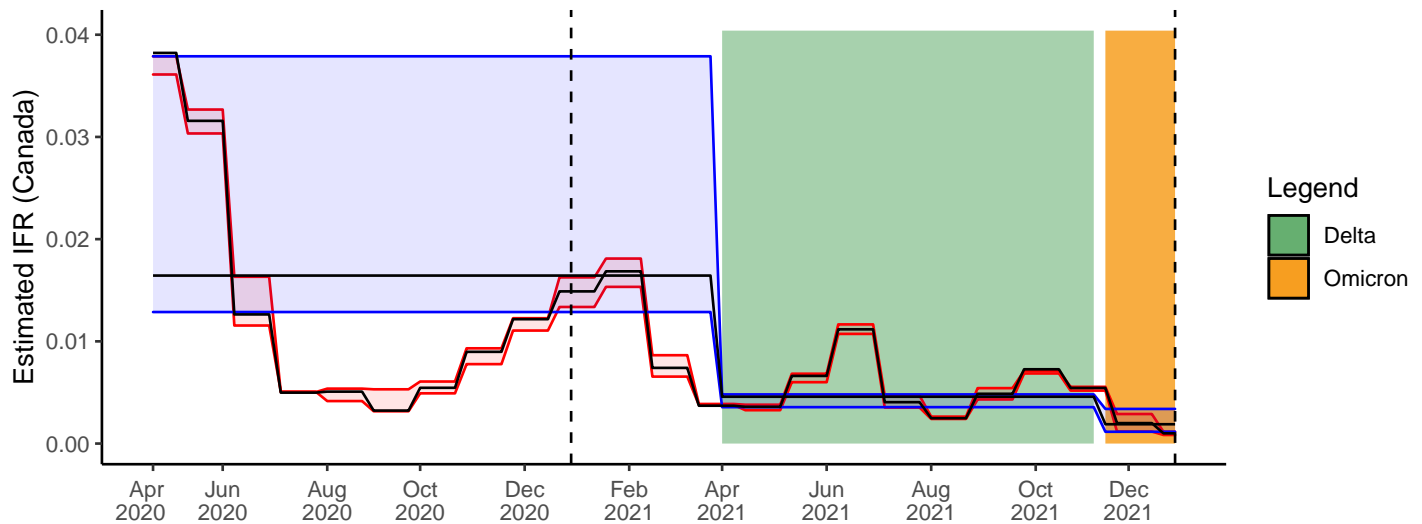
Figure 5: Estimated infection fatality rate (IFR) for COVID-19 infections within Canada. The time periods for the two variants of concern Delta and Omicron are depicted with coloured bands. The estimated IFR for each time period is 0.015 (early pandemic period), 0.005 (Delta period), and 0.002 (Omicron period). The two vertical dashed lines indicate 1 Jan 2021 and 1 Jan 2022. Bands show 95% credible intervals. The red shows monthly estimates, while the blue shows estimates for each of the three time periods.

important to note that while γ is an identifiable parameter in the model, γ measures average linear growth in cases, and so is not necessarily the true importation rate. Rather, the very large γ estimate for Quebec could indicate better control of the exponential spread rate due to quarantines and other public health measures. Evidence for this can be seen in Figure 4, where the domestic spread rate among undetected cases for Quebec is much lower than for the other provinces.

To estimate the infection fatality rate (IFR) for Canada as a whole, we used the estimated new cases, $\widehat{S}_{it} + \widehat{G}_{it}$ per time period P, then we estimated the IFR as $\widehat{IFR}_P = \sum_{i,t \in P} D_{it} / \sum_{i,t \in P} \widehat{S}_{it} + \widehat{G}_{it}$. The estimated IFRs for Canada as a whole with 95% credible intervals are: 0.015 (0.012, 0.038) for the early pandemic period, 0.005 (0.004, 0.006) for the Delta period, and 0.002 (0.001, 0.003) for the Omicron period (Figure 5).

3.2 Case Study: British Columbia

3.2.1 Data Sources

We used several publicly available sources to compile the data for our B.C. case study. The B.C. Surveillance Reports (BC Centre for Disease Control, 2020) were used to gather counts of cases, recoveries, and deaths. These data are shown for each Health Authority region in Figure S8 in the Appendix. Province of B.C. laboratory data (Province of British Columbia, 2020) was used as a source for COVID-19 testing volumes per region. Start dates for the Phases of the B.C. Recovery plan were obtained from the Government of B.C. emergency preparedness response web pages (Government of British Columbia, 2020).

Data for this B.C. case study was limited to the date range 2 Apr 2020 (Week 1) to 30 Oct 2020 (Week 31). After this period, the B.C. Surveillance Reports began to exclude the data necessary for fitting these models (case counts, case recoveries, and deaths split by Health Authority region). These methods could be easily

applied to more recent pandemic data if the required aggregate data were made publicly available.

3.2.2 Parameter Covariates

In this case study we explored many combinations of parameter covariates in order to better understand our model, and to investigate the relationships between the covariates and the data. Health Authority Region (denoted *reg*) was used as a covariate for both λ and γ in all of our considered models. The covariate *reg* was also used for ω_1 and ω_2 in several models to indicate region dependency. Phase of the B.C. Recovery Plan (denoted *pha*) was also considered as a potential covariate for γ, ω_1 and ω_2, to indicate that the parameters change with time at the boundary of the recovery plan phases. For detection probability *p*, we considered the parameter covariates: *reg*, *pha*, COVID-19 testing volume (*vol*), and a baseline offset which was constant across regions (B).

3.2.3 Model Selection

We used the widely applicable information criterion (WAIC: Watanabe and Opper, 2010) to aid in model selection and study the impact of covariates. Gelman et al. (2014) discuss the limitations of relying solely on log predictive density methods (such as WAIC) for model selection. In particular, the authors note that such model selection procedures can over fit the model to the data, providing suboptimal predictive performance. To that end, they caution to view information criteria as an approach to understand fitted models rather than to choose from among them.

While we do use WAIC to aid in model selection, it is not the sole criteria. For example, we select the second best performing model according to WAIC as our preferred model. We did this for three reasons: (1) the top two ranked models perform very similarly in terms of estimated latent variables, (2) the number of model parameters is far less for the second ranked model, and (3) the covariates used in the second model carry far more explanatory value than those in the first ranked model.

3.2.4 Results

Our results for fitting 22 models with different organizations of the covariates and conditions on ω to the B.C. data are summarized in Table S5 in the Appendix. Model M1 performed best in terms of WAIC, and model M22 performed worst (we label the models in descending order of WAIC). Excluding the four models which used no covariates for ω_1 and ω_2, every model for which ω_1 was allowed to differ from ω_2 performed better than the models which forced $\omega_1 = \omega_2$. This is strong evidence in favour of the models which allow the domestic spread rate to be affected by detection status, since those models perform uniformly better in terms of WAIC. In addition, every model that allowed ω_1 and ω_2 to vary with Phase performed better than models not varying with Phase. This suggests spread rates were not constant over the course of the early pandemic.

We identify model M2 as the best model, despite M1 having the lower WAIC score. Figure S9 in the Appendix compares the estimated active cases for each Health Authority region between model M1 and model M2. The two models perform similarly for all sites, except Fraser Health Authority region, for which the model M2 predicts a substantially larger initial number of active cases. However, model M1 uses 18 more parameters than model M2, and so is at greater risk of overfitting. Model M2 uses testing volume as a covariate for detection probability, which is far more interpretable than B.C. Recovery Plan Phase (which is used instead
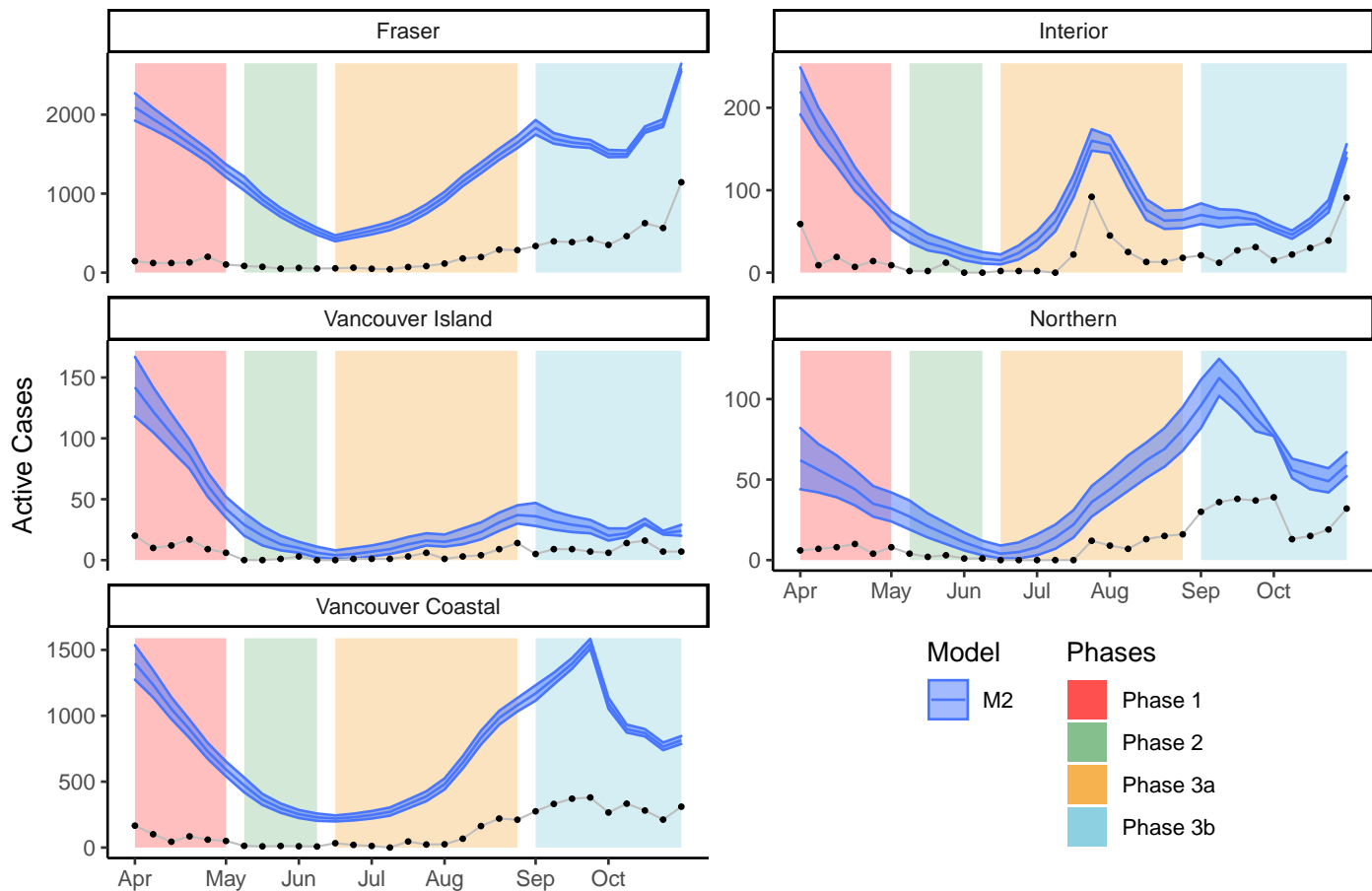
Figure 6: Plots of active cases split by Health Authority Region. Data starts on 2 Apr 2020 (Week 1) and ends on 30 Oct 2020 (Week 31). The blue bands show the 95% credible intervals for total active cases as estimated using model M2. The black dotted line shows the newly detected active cases each week.

for model M1, and is correlated with many confounding factors such as season, health mandates, and human mobility). Figure S9 also compares the results for the five single-site models (shown in green) against the two best fitted multi-site models (M1 in red and M2 in blue). The single-site models show larger uncertainty in their estimates through wide credible intervals, illustrating an advantage of using multi-site modelling.

We show the results for our chosen model M2 in Figure 6. The trend for all regions over this period of study was for a large initial number of active cases, which falls off leading up to week 10, and builds leading into the later stages of the 31 week period. All five regions showed signs of peaking at different times between weeks 17 and 26, with a second peak beginning around week 30, and likely continuing after this period of study.

3.3 Comparing Results

We compare results between three case studies overlapping in time intervals and regions to illustrate several important points. Model tails (time periods near the beginning and the end of the study) are less accurate, due to a lack of information outside of the study time boundaries (Section 3.3.1). This is particularly important to note when interpreting our Canada case study results. Since the Omicron time period lies on the boundary, there is less certainty in our estimates for that time period. Future applications of these methods should be

aware of these boundary limitations, and should not put excessive weight on estimates near the study time boundaries. Another important point is the dependence of these models on data quality. The difference in case counts between the BCCDC Surveillance reports and the PHAC situation reports impacts the estimates of total active cases (see Figure S10 in the Appendix). However, when the data sources are the same, the multi-site models produce more precise estimates than the single-site models (Section 3.3.2). Therefore, when using these models it is important to use the most accurate and highest quality case count data available.

3.3.1 British Columbia Comparison

Figure S10 in the Appendix illustrates the estimated total cases in B.C. as estimated by the single-site Health Authority Region model (green), and as estimated by the multi-site Canada case study model (blue). The two models diverge considerably in estimated total cases in both tails, while agreeing in the middle period. There are several reasons for this. First, the data used to fit the models is not the same. The detected case counts are a form of administrative data, and have been updated and corrected over time, and the counts used in the Canada model are likely to be more accurate than the counts used in the B.C. model (Figure S10). Second, the Canada model has no covariate equivalent to the B.C. Recovery Plan phases covariate of the B.C. model, thus the B.C. model allows for more granular changes in dynamics. Third, the Canada model pools information from the pandemic across Canada, allowing the province and territory estimates to be informed by national trends. Fourth, the Canada model is trained on 90 weeks of data rather than 31, and over 13 sampling sites rather than 5. The larger amount of data used for the Canada-wide model means its results are likely to be more accurate. Fifth, the B.C. model begins with three earlier weeks of data, so that the beginning tail of the model is likely more accurate than the Canada model. Conversely, the Canada model contains 62 weeks of more recent data than the B.C. model, meaning the end tail of the Canada model is likely to be more accurate.

3.3.2 Northern Health Authority Comparison

We compare the Northern Health Authority Region results from the single-site model of Parker et al. (2021) with results from our multi-site model M2 (Figure 7). The single-site results were obtained using maximum likelihood methods, and so the variability shown indicates the 95% confidence interval, whereas the multi-site model uses Bayesian MCMC to obtain 95% credible intervals. The two models show excellent agreement through overlapping credible/confidence bands, and share a common maximum during week 24, but the multi-site model has increased precision over the single-site model. An important advantage to the Bayesian MCMC method of model fitting is the ability to estimate active cases even during periods when no new cases are detected, as was the case for the Northern Health region during weeks 13 through 16.

4   Discussion

Throughout the pandemic, case counts have been only a lower bound on the total number of active infections. Our Canada case study estimates the levels of under-reporting for each province and territory. Estimates of total active infections vary widely in magnitude across Canada and over time, with over 200,000 concurrent active cases at times in Ontario and Quebec, and under 400 concurrent active cases at any time in Nunavut. Our results show that although the first confirmed infection in Nunavut occurred in October 2020, it is likely
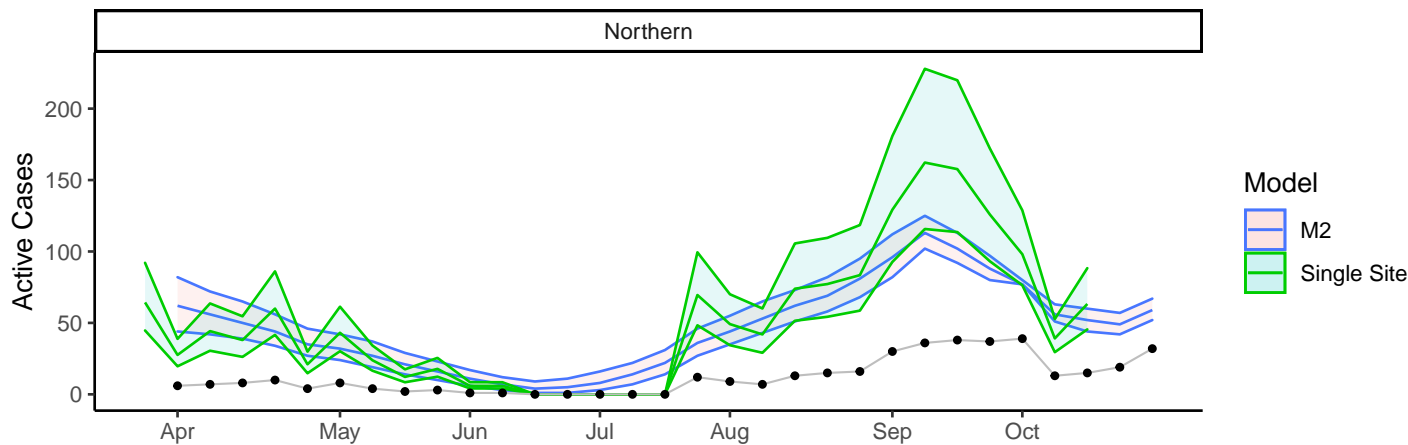
Figure 7: Plot of active cases for the Northern Health Authority region. Data starts on 2 Apr 2020 (Week 1) and ends on 30 Oct 2020 (Week 31). The blue band shows the 95% credible interval for total active cases as estimated using model M2. The green bands show the 95% confidence intervals for total active cases as estimated using the single site model from Parker et al. (2021), denoted Single Site. The black dotted line shows the newly detected active cases each week.

that there were over 100 active infections in Nunavut at that time, and that the first infection likely would have occurred between June and August 2020.

Our estimates for detection probability show that there were similar detection levels across Canada. In the early pandemic, most provinces/territories had very low testing volumes (less than 10 tests per 1000 population size), which led to low detection rates (under 20% detection for most provinces/territories). Among the provinces, Prince Edward Island had the highest minimum detection rate (30%), while Newfoundland and Labrador had the lowest (3%). Among the territories, Northwest Territories had the highest minimum detection rate (20%), while Nunavut had the lowest (2%). Testing volume is not the only factor in determining detection, as can be seen by comparing the results from Ontario with those from Quebec (Figure 3). Both provinces had very similar testing volumes throughout the pandemic; however, the detection rate was substantially higher in Ontario than in Quebec. Ontario had a low of 27% and a high of 64%, compared with Quebec's low of 10% and high of 52%. The reason for this is unclear. It could be due to differences in testing protocols, differences in access to testing, geographic or political differences, or many other possible factors. Future research into the effects of public messaging and health policies on detection rates would be beneficial and could improve our understanding of this phenomenon.

In Canada, the case-fatality rate for COVID-19 was estimated to be 4.9% in April 2020 (Abdollahi et al., 2020), and 3.36% by the end of 2020 (Shim, 2021). However, CFR is larger than IFR when there are undetected cases. Understanding the IFR during recent periods of the pandemic allows us to understand the personal risk associated with contracting SARS-CoV-2. We estimated the weekly probability of death p_d over the course of the pandemic, and found that for all provinces and territories of Canada the mortality rates have decreased over time. In general, mortality rates decreased with increased rate of first vaccination dose (Figure S12 in the Appendix), increased during the Delta time period, and decreased again in the Omicron time period. Weekly probability of death is different from overall probability of death, which is better measured through IFR. The weekly probability of death is the average probability of an active case dying during a particular week (if they

neither die nor recover during that week, then they will have a further chance of dying in the following week and so on until they either recover or die). IFR is a more easily interpreted measure of mortality rates than p_d, since IFR is the overall mortality rate for infected individuals. Previous findings regarding IFR using data across 15 countries determined it likely that IFR for COVID-19 was $< 0.2\%$ (Ioannidis et al., 2020). Fisman et al. (2020) estimated the overall IFR in Ontario to be 0.8% (0.75%, 0.85%), with a large range based on age (from 0.01% up to 12.7%). Our findings indicate that short term estimates of IFR (such as our monthly estimates in Figure 5) can fluctuate rapidly over time. Our estimate for the early pandemic time period of 1.5% is much higher than the 0.2% from Ioannidis et al. (2020). However, our monthly estimates show that depending on which month of data is considered, estimates of IFR would have varied from a high of nearly 4% down to a low of 0.3%. Our estimates for the Delta and Omicron periods are more moderate at 0.5% and 0.2%, respectively.

Estimates of recovery probability are useful for understanding the length of an average infection. During the early pandemic period the weekly probability of recovery was 35.0%, and the weekly probability of remaining an active case was 64.7%. This implies that the average recovery time and 95% recovery interval was 11.3 (6.1, 15.4) days (obtained by solving the simple geometric series in p_a, see Appendix S.3). For the Delta and Omicron periods, the average recovery time was 8.5 (6.0, 12.8) days and 14.0 (6.1,17.0) days, respectively. We see the average recovery time increased during the Omicron period, while the lower bound on recovery time has remained around 6 days throughout the pandemic.

According to the National Collaborating Centre for Infectious Diseases (2022), both the Delta and Omicron variants of concern have been found to be more transmissible than the earlier variants. Thus we would expect to find an increased ω_1 and ω_2 during those time periods. Our Canada model agrees with this expectation (Figure 4), where domestic spread rates are seen to increase across Canada at the Delta boundaries as well as at the Omicron boundaries. A single vaccine dose is correlated with decreased spread rate for the undetected cases (corresponding loosely to asymptomatic, pre-symptomatic, and low severity cases), and is correlated with increased spread rate for the detected cases (corresponding loosely to symptomatic and medium to high severity cases). The increased spread rate could be explained by decreases in severity for vaccinated individuals (Lauring et al., 2022), so that the detected cases are more inclined to mobility and interaction events, as well as relaxed health measures correlated with increasing vaccination rates. Receiving a second vaccine dose is correlated with an increase in spread rate for undetected cases, which may be explained by a decrease in perceived personal danger from contracting the disease when vaccinated with two doses. The second vaccine dose is correlated with a large decrease in spread rate for the detected cases in all provinces, but not in the territories.

Our British Columbia case study was limited in scope by a lack of available public data after 30 Oct 2020. For future pandemics and disease outbreaks, we would urge all public health authorities (in B.C., in Canada, and abroad) to make weekly aggregate counts of cases, recoveries, and deaths publicly accessible as early as possible to promote greater knowledge and more expedient research. The decision to do so can in turn lead to better informed, more timely health policy decision making, which can save lives and reduce the burden on our health care systems.

Acknowledgments

References

Elaheh Abdollahi, David Champredon, Joanne M. Langley, Alison P. Galvani, and Seyed M. Moghadas. Temporal estimates of case-fatality rate for COVID-19 outbreaks in Canada and the United States. *Canadian Medical Association Journal*, 192(25):E666–E670, 2020.

Muluneh Alene, Leltework Yismaw, Moges Agazhe Assemie, Daniel Bekele Ketema, Belayneh Mengist, Bekalu Kassie, and Tilahun Yemanu Birhan. Magnitude of asymptomatic COVID-19 cases throughout the course of infection: A systematic review and meta-analysis. *PLOS ONE*, 16(3):e0249090, 2021.

Jennifer A. Appleby, Nathan King, Kate E. Saunders, Anne Bast, Daniel Rivera, Jin Byun, Simone Cunningham, Charandeep Khera, and Anne C. Duffy. Impact of the COVID-19 pandemic on the experience and mental health of university students studying in Canada and the UK: A cross-sectional study. *BMJ Open*, 12(1):e050187, 2022.

Yusha Araf, Fariya Akter, Yan-dong Tang, Rabeya Fatemi, Md Sorwer Alam Parvez, Chunfu Zheng, and Md. Golzar Hossain. Omicron variant of SARS-CoV-2: Genomics, transmissibility, and responses to current COVID-19 vaccines. *Journal of Medical Virology*, 94(5):1825–1832, 2022.

Richard J. Barker, Matthew R. Schofield, William A. Link, and John R. Sauer. On the reliability of N-mixture models for count data. *Biometrics*, 74(1):369–377, 2018.

BC Centre for Disease Control. BC COVID-19 data [surveillance reports]. Retrieved from `http://www.bccdc.ca/health-info/diseases-conditions/covid-19/data`, 2020. Accessed Spring 2022.

Daniel Béland, Shannon Dinan, Philip Rocco, and Alex Waddan. Social policy responses to COVID-19 in Canada and the United States: Explaining policy variations between two liberal welfare state regimes. *Social Policy & Administration*, 55(2):280–294, 2021.

Eran Bendavid, Bianca Mulaney, Neeraj Sood, Soleil Shah, Rebecca Bromley-Dulfano, Cara Lai, Zoe Weissberg, Rodrigo Saavedra-Walker, Jim Tedrow, Andrew Bogan, Thomas Kupiec, Daniel Eichner, Ribhav Gupta, John P. A. Ioannidis, and Jay Bhattacharya. COVID-19 antibody seroprevalence in Santa Clara County, California. *International Journal of Epidemiology*, 50(2):410–419, 2021.

Diana Buitrago-Garcia, Dianne Egli-Gany, Michel J. Counotte, Stefanie Hossmann, Hira Imeri, Aziz M. Ipekci, Georgia Salanti, and Nicola Low. Occurrence and transmission potential of asymptomatic and presymptomatic SARS-CoV-2 infections: A living systematic review and meta-analysis. *PLOS Medicine*, 17(9):e1003346, 2020.

Vinay K. R. Chimmula and Lei Zhang. Time series forecasting of COVID-19 transmission in Canada using LSTM networks. *Chaos, Solitons & Fractals*, 135:109864, 2020.

Master R. O. Chisale, Sheena Ramazanu, Saul Eric Mwale, Pizga Kumwenda, Mep Chipeta, Atipatsa C. Kaminga, Obed Nkhata, Billy Nyambalo, Elton Chavura, and Balwani C. Mbakaya. Seroprevalence of anti-SARS-CoV-2 antibodies in Africa: A systematic review and meta-analysis. *Reviews in Medical Virology*, 32(2):e2271, 2022.

Brigitte S. Cypress. COVID-19: The economic impact of a pandemic on the healthcare delivery system in the United States. *Nursing Forum*, 57(2):323–327, 2022.

David Dail and Lisa Madsen. Models for estimating abundance from repeated counts of an open metapopulation. *Biometrics*, 67(2):577–587, 2011.

Perry de Valpine, Daniel Turek, Christopher Paciorek, Cliff Anderson-Bergman, Duncan Temple Lang, and Ras Bodik. Programming with models: Writing statistical algorithms for general model structures with NIMBLE. *Journal of Computational and Graphical Statistics*, 26(2):403–413, 2017.

Perry de Valpine, Christopher Paciorek, Daniel Turek, Nick Michaud, Cliff Anderson-Bergman, Fritz Obermeyer, Claudia Wehrhahn Cortes, Abel Rodrìguez, Duncan Temple Lang, and Sally Paganin. *NIMBLE: MCMC, Particle Filtering, and Programmable Hierarchical Modeling*, 2021. URL `https://cran.r-project.org/package=nimble`. R package version 0.11.1.

Emily B. Dennis, Byron J. T. Morgan, and Martin S. Ridout. Computational aspects of N-mixture models. *Biometrics*, 71 (1):237–246, 2015.

Zachary Desson, Emmi Weller, Peter McMeekin, and Mehdi Ammi. An analysis of the policy responses to the COVID-19 pandemic in France, Belgium, and Canada. *Health Policy and Technology*, 9(4):430–446, 2020.

Ensheng Dong, Hongru Du, and Lauren Gardner. An interactive web-based dashboard to track COVID-19 in real time. *The Lancet Infectious Diseases*, 20(5):533–534, 2020.

Brendan P. Dougherty, Ben A. Smith, Carolee A. Carson, and Nicholas H. Ogden. Exploring the percentage of COVID-19 cases reported in the community in Canada and associated case fatality ratios. *Infectious Disease Modelling*, 6: 123–132, 2021.

David J. A. Dozois. Anxiety and depression in Canada during the COVID-19 pandemic: A national survey. *Canadian Psychology/Psychologie canadienne*, 62(1):136–142, 2021.

Daniel R. Feikin, Marc-Alain Widdowson, and Kim Mulholland. Estimating the percentage of a population infected with SARS-CoV-2 using the number of reported deaths: A policy planning tool. *Pathogens*, 9(10):838, 2020.

Amanda Fernández-Fontelo, David Moriña, Alejandra Cabaña, Argimiro Arratia, and Pere Puig. Estimating the real burden of disease under a pandemic situation: The SARS-CoV2 case. *PLOS ONE*, 15(12):e0242956, 2020.

David N. Fisman, Steven J. Drews, Ashleigh R. Tuite, and Sheila F. O'Brien. Age-specific SARS-CoV-2 infection fatality and case identification fraction in Ontario, Canada. *medRxiv preprint 2020.11.09.20223396*, 2020.

Andrew Gelman, Jessica Hwang, and Aki Vehtari. Understanding predictive information criteria for Bayesian models. *Statistics and Computing*, 24(6):997–1016, 2014.

Government of British Columbia. Phase 1: BC's restart plan. Retrieved from `https://www2.gov.bc.ca/gov/content/safety/emergency-preparedness-response-recovery/covid-19-provincial-support/phase-1`, 2020. Accessed Fall 2020.

Government of Canada. COVID-19 daily epidemiology update. Retrieved from `https://health-infobase.canada.ca/covid-19/epidemiological-summary-covid-19-cases.html`, 2022a. Accessed Spring 2022.

Government of Canada. COVID-19 vaccination in Canada. Retrieved from `https://health-infobase.canada.ca/covid-19/vaccination-coverage/`, 2022b. Accessed Spring 2022.

Government of Yukon. COVID-19 data dashboard. Retrieved from `https://covid-19-data-dashboard.serv ice.yukon.ca/`, 2022. Accessed Spring 2022.

Rrezart Halili, Jeta Bunjaku, Bujar Gashi, Teuta Hoxha, Agron Kamberi, Nexhmedin Hoti, Riaz Agahi, Vlora Basha, Visar Berisha, and Ilir Hoxha. Seroprevalence of anti-SARS-CoV-2 antibodies among staff at primary healthcare institutions in Prishtina. *BMC Infectious Diseases*, 22(1):57, 2022.

Tasnim Hasan, Thach Ngoc Pham, Thu Anh Nguyen, Thu Le Hien Thi, Van Le Duyet, Thi Dang Thuy, Trang Dinh Van, Yen Ngoc Pham, Ha Viet Nguyen, Giang Linh Tran, Van Thi Cam Nguyen, Thanh Trung Nguyen, Viet Quang Truong, Than Huu Dao, Chung Thanh Le, Nam Tan Truong, Hoang Trung Vo, Phuc Thanh Le, Thao Thanh Nguyen, Vinh Van Luu, Vinh Dai Nguyen, Brett G. Toelle, Guy B. Marks, and Greg J. Fox. Sero-prevalence of SARS-CoV-2 antibodies in high-risk populations in Vietnam. *International Journal of Environmental Research and Public Health*, 18(12):6353, 2021.

Jingjing He, Yifei Guo, Richeng Mao, and Jiming Zhang. Proportion of asymptomatic coronavirus disease 2019: A systematic review and meta-analysis. *Journal of Medical Virology*, 93(2):820–830, 2021.

Xi Huo, Jing Chen, and Shigui Ruan. Estimating asymptomatic, undetected and total cases for the COVID-19 outbreak in Wuhan: A mathematical modeling study. *BMC Infectious Diseases*, 21(1):476, 2021.

John P. A. Ioannidis, Cathrine Axfors, and Despina G. Contopoulos-Ioannidis. Population-level COVID-19 mortality risk for non-elderly individuals overall and for non-elderly individuals without underlying diseases in pandemic epicenters. *Environmental Research*, 188:109890, 2020.

Fredrik Kahn, Carl Bonander, Mahnaz Moghaddassi, Magnus Rasmussen, Ulf Malmqvist, Malin Inghammar, and Jonas Björk. Risk of severe COVID-19 from the Delta and Omicron variants in relation to vaccination status, sex, age and comorbidities—surveillance results from southern Sweden, July 2021 to January 2022. *Eurosurveillance*, 27(9): 2200121, 2022.

Adam S. Lauring, Mark W. Tenforde, James D. Chappell, Manjusha Gaglani, Adit A. Ginde, Tresa McNeal, Shekhar Ghamande, David J. Douin, H. Keipp Talbot, Jonathan D. Casey, Nicholas M. Mohrand Anne Zepeski, Nathan I. Shapiro, Kevin W. Gibbs, D. Clark Files, David N. Hager, Arber Shehu, Matthew E. Prekker, Heidi L. Erickson, Matthew C. Exline, Michelle N. Gong, Amira Mohamed, Nicholas J. Johnson, Vasisht Srinivasan, Jay S. Steingrub, Ithan D. Peltan, Samuel M. Brown, Emily T. Martin, Arnold S. Monto, Akram Khan, Catherine L. Houghand Laurence W. Busse, Caitlin C. ten Lohuis, Abhijit Duggal, Jennifer G. Wilson, Alexandra June Gordon, Nida Qadir, Steven Y. Chang, Christopher Mallow, Carolina Rivas, Hilary M. Babcockand Jennie H. Kwon, Natasha Halasa, Carlos G. Grijalva, Todd W. Rice, William B. Stubblefield, Adrienne Baughman, Kelsey N. Womack, Jillian P. Rhoads, Christopher J. Lindsell, Kimberly W. Hart, Yuwei Zhu, Katherine Adams, Stephanie J. Schrag, Samantha M. Olson, Miwako Kobayashi, Jennifer R. Verani, Manish M. Patel, and Wesley H. Self. Clinical severity of, and effectiveness of mRNA vaccines against, COVID-19 from Omicron, Delta, and Alpha SARS-CoV-2 variants in the United States: Prospective observational study. *British Medical Journal*, 376:e069761, 2022.

Chunyu Li, Yuchen Zhu, Chang Qi, Lili Liu, Dandan Zhang, Xu Wang, Kaili She, Yan Jia, Tingxuan Liu, Daihai He, Momiao Xiong, and Xiujun Li. Estimating the prevalence of asymptomatic COVID-19 cases and their contribution in transmission—using Henan Province, China, as an example. *Frontiers in Medicine*, 8:591372, 2021.

Rashidul Alam Mahumud, Mohammad Afshar Ali, Satyajit Kundu, Md Ashfikur Rahman, Joseph Kihika Kamara, and Andre M. N. Renzaho. Effectiveness of COVID-19 vaccines against Delta variant (B.1.617.2): A meta-analysis. *Vaccines*, 10(2):277, 2022.

Muhammad Abu Shadeque Mullah and Ping Yan. A semi-parametric mixed model for short-term projection of daily COVID-19 incidence in Canada. *Epidemics*, 38:100537, 2022.

National Collaborating Centre for Infectious Diseases. Updates on COVID-19 variants of concern (VOC). Retrieved from `https://nccid.ca/covid-19-variants/`, 2022. Accessed Spring 2022.

Matthew R. P. Parker, Yangming Li, Lloyd T. Elliott, Junling Ma, and Laura L. E. Cowen. Under-reporting of COVID-19 in the Northern Health Authority region of British Columbia. *Canadian Journal of Statistics*, 49(4):1018–1038, 2021.

Province of British Columbia. BC COVID-19—Laboratory information. Retrieved from `https://governmentofbc .maps.arcgis.com/home/item.html?id=\ba047e4a9bd24beb9ca6e94c05eddef9`, 2020. Accessed Spring 2021.

R Core Team. *R: A Language and Environment for Statistical Computing*. R Foundation for Statistical Computing, Vienna, Austria, 2022. `https://www.r-project.org/`.

J. Andrew Royle. N-mixture models for estimating population size from spatially replicated counts. *Biometrics*, 60(1): 108–115, 2004.

Sahar Saeed, Steven J. Drews, Chantale Pambrun, Qi-Long Yi, Lori Osmond, and Sheila F. O'Brien. SARS-CoV-2 seroprevalence among blood donors after the first COVID-19 wave in Canada. *Transfusion*, 61(3):862–872, 2021.

Eunha Shim. Regional variability in COVID-19 case fatality rate in Canada, February–December 2020. *International Journal of Environmental Research and Public Health*, 18(4):1839, 2021.

Rahul Subramanian, Qixin He, and Mercedes Pascual. Quantifying asymptomatic infection and transmission of COVID-19 in New York City using observed cases, serology, and testing capacity. *Proceedings of the National Academy of Sciences*, 118(9):e2019716118, 2021.

Satoshi Tanaka. Economic impacts of SARS/MERS/COVID-19 in Asian countries. *Asian Economic Policy Review*, 17 (1):41–61, 2022.

Ashleigh R. Tuite, David N. Fisman, and Amy L. Greer. Mathematical modelling of COVID-19 transmission and mitigation strategies in the population of Ontario, Canada. *Canadian Medical Association Journal*, 192(19):E497–E505, 2020.

Sumio Watanabe and Manfred Opper. Asymptotic equivalence of Bayes cross validation and widely applicable information criterion in singular learning theory. *Journal of Machine Learning Research*, 11(10):3571–3594, 2010.

Karl Weiss, Taghi M. Khoshgoftaar, and DingDing Wang. A survey of transfer learning. *Journal of Big Data*, 3(1):9, 2016.

Kate Zinszer, Britt McKinnon, Noémie Bourque, Laura Pierce, Adrien Saucier, Alexandra Otis, Islem Cheriet, Jesse Papenburg, Marie Ève Hamelin, Katia Charland, Julie Carbonneau, Monica Zahreddine, Ashley Savard, Geneviève Fortin, Alexander Apostolatos, Nacy Haley, Nathalie Ratté, Isabel Laurin, Cat Tuong Nguyen, Patricia Conrod, Guy Boivin, Gaston De Serres, and Caroline Quach. Seroprevalence of SARS-CoV-2 antibodies among children in school and day care in Montreal, Canada. *JAMA Network Open*, 4(11):e2135975, 2021.

Supplementary Material

S.1 Single-Site Model

Here we describe the mathematical structure of the single-site model. We drop the site subscript i from the multi-site model to produce the single-site model. Our model makes use of three sets of reported data: The observed case counts $\{n_t\}$, the recoveries among case counts $\{r_t\}$, and the deaths due to the disease $\{D_t\}$. This description mirrors the multi-site model from Section 2.1, but with some simplifications due to the dropped subscript.

(1)   Initial Abundance: $N_1 \sim \text{Poisson}(\lambda)$
(2)   State Process: $\{A_t, D_t, R_t\} \sim \text{Multinomial}(N_t; p_a, p_d, p_r)$
(3)   Observed Active Cases: $a_t = n_t + a_{t-1} - r_{t-1} - d_{t-1}, a_0 = 0$
(4)   Domestic Spread: $S_t \sim \text{Poisson}(\Omega_{t-1})$, for $t > 1$
(5) Ω_{t-1} : $\omega_1(N_{t-1} - a_{t-1}) \cdot \delta + \omega_2 a_{t-1}$
(6) δ : $(H - N_t)/H$, where H is total population size
(7)   Imported Cases: $G_t \sim \text{Poisson}(\gamma)$, for $t > 1$
(8)   Abundance Updates: $N_t = A_{t-1} + S_t + G_t$, for $t > 1$
(9)   Observation Process I: $n_t \sim \text{Binomial}(N_t - a_{t-1}, p)$
(10) Observation Process II: $\{a_t - d_t - r_t, d_t, r_t\} \sim \text{Multinomial}(a_t; p_a^*, \alpha p_d, p_r)$

(1) The initial abundance. N_t is the total (unknown) number of active cases at time t. N_1 is the initial number of active cases at time $t = 1$. The parameter λ is the expected initial number of cases.

(2) The multinomial state process. Each active case in N_t is partitioned at time t into one of three categories according to whether the case will remain active, die, or recover by time $t + 1$. A_t is the subset of N_t which remains active (with probability p_a). D_t is the subset of N_t which will die (with probability p_d). R_t is the subset of N_t which will recover (with probability p_r). The parameter p_a is determined, since $p_a = 1 - p_r - p_d$.

(3) The observed active cases a_t is a deterministic quantity, specified by the observed data. It is the number of observed cases which are still active at time t. a_t is calculated recursively, with a_0, r_0, d_0, n_0 all zero by definition, unless observed active cases are known for the previous time period, in which case a_0 would not be zero. Note that if deaths were fully observed, d_t would be equal to D_t.

(4) S_t models the domestic spread, which is the spread of the disease due to contact with infectious individuals within the population. Ω_t is the average number of new infections per time interval, which is calculated using the two parameters ω_1 and ω_2. S_t allows for exponential growth of cases, but does not allow for a spontaneous outbreak within a population that has zero active cases.

(5) Ω_t has a similar meaning to the reproductive number R_0. However, unless the time interval is the same as the infectious period, Ω_t is in general different from R_0. The parameter ω_1 is the average new infections per unobserved active case $N_{t-1} - a_{t-1}$. The parameter ω_2 is the average number of new infections per observed active case a_{t-1}.

(6) δ is a moderating term which modulates the growth of cases as the population becomes saturated with cases. H is the total population size of the region, which is the maximum number of infected individuals that

are possible. δ decreases to zero linearly as N_t approaches H. Thus, the spread rate goes to zero as the population becomes saturated with cases (we assume that the spread rate is proportional to the number of susceptible individuals).

(7) G_t models the number of imported cases, which are new cases entering the population (from travel for example). The parameter γ is the average number of new imported cases per time interval. Imported cases allow for disease to occur even when $N_1 = 0$. This can allow for spontaneous outbreaks in regions with no previous active cases. G_t allows for linear growth of cases over time.

(8) The abundance updates. Because we assume that the number of cases changes with time, we calculate the abundance after time 1 using A_t from the state process in addition to the growth terms S_t and G_t. In this way, N_t are previous cases which have remained active (A_{t-1}) plus the new cases due to domestic spread (S_t) and the new cases due to importation (G_t).

(9) The first observation process models the reporting of case counts. The parameter p is the probability of detecting a case, and so $1 - p$ gives the under-reporting rate. The usual N-mixture model would have $n_t \sim \text{Binomial}(N_t, p)$. However, since N_t is the total number of active cases, this would allow double counting (because observed cases n_t are tracked until recovery or death). Instead, we subtract the already observed active cases prior to the binomial thinning: $N_t - a_{t-1}$.

(10) The second observation process models reporting of recoveries and deaths. Similar to the state process for N_t, the states a_t are partitioned into cases that remain active, cases that die, and cases that recover. If deaths are assumed fully detected, $\alpha = 1/p$ would account for perfect detection of deaths (which increases the proportion of observed deaths among detected cases unless $p = 1$), and we would set d_t to D_t where appropriate. In the situation where deaths are under-reported, we would set $\alpha = 1$. The parameter p_a^* is determined for the same reason that p_a is determined.

The single-site model contains seven estimable model parameters: λ, p, p_r, p_d, γ, ω_1, and ω_2. It contains three sets of observed data: $\{n_t\}$, $\{d_t\}$, $\{r_t\}$. And it contains six sets of latent variables: $\{N_t\}$, $\{D_t\}$, $\{R_t\}$, $\{A_t\}$, $\{S_t\}$, $\{G_t\}$. In the situation where deaths are fully observed, such as in our two case studies, $\{D_t\}$ is no longer a latent variable, and replaces $\{d_t\}$ as observed data. This model is an extension and major update to the single-site model from Parker et al. (2021).

S.2   Simulations

We conduct simulations to investigate the identifiability of all parameters. This is particularly important for the parameter ω_1 which is only implicity tied to the data $\{n_{it}\}$ through the unobserved quantities $\{N_{it}\}$. We set the number of sampling sites to be 2 and the number of sampling occasions to be 30. We chose one set of ground truth parameter values for this simulation: $\lambda = 50$, $\gamma = 5$, $\omega_1 = 0.25$, $\omega_2 = 0.5$, $p_r = 0.4$, $p_d = 0.1$, $p = 0.7$.

The parameter values for the simulation were chosen to be of reasonable magnitude, and to avoid parameter boundaries. We chose λ to be 50 to avoid the slow pandemic start situation of $\lambda = 0$, which could cause the initial few time steps to have no new cases except through importation, until enough cases existed for domestic spread to take hold. We chose γ to be an appreciable fraction of λ so that linear growth would be immediately impactful to the growth of case counts. A smaller γ would likely incur larger variance in the

posterior distributions for γ. We chose to have ω_1 and ω_2 set between 0 and 1 to produce moderate spread rates, and we chose for them to be different from each other in order to test their identifiability. We chose p_r to be 0.4 as that was expected to be close to the actual recovery probability for Canada. We chose p_d to be 0.1 so that the number of deaths would be small but appreciable for the simulation study. The choice of $p = 0.7$ was arbitrary, and away from zero or 1 (which may be corner cases and which are unrealistic). In particular $p = 1$ would imply that every case was identified at all times. This is unreasonable even if a population census was performed at each time step, since it would also require perfect testing results. Similarly, $p = 0$ would imply that all case counts were zero for every time step, which would mean there were no data available at all. The value $p = 0.7$ was chosen as a reasonable guess as to the maximum probability of detection across Canada.

Our simulation consisted of 50 runs. For each run a random set of population data $(\{n_{it}\}, \{r_{it}\}, \{D_{it}\})$ was generated using the model definition. The data generating algorithm is shown in Listing S1. We chose to use two sampling sites and thirty sampling occasions for the simulation. The model was then fit to the generated data using Bayesian MCMC with a burnin of 100,000, thinning of 200, for a total of 4,500 iterations after burn-in and thinning. The resulting posterior means were collected for each parameter. The simulation results are shown in Figure S8, along with the prior distributions chosen for each parameter. Each parameter was found to be identifiable (Figure S8). The parameter with the least degree of certainty (as indicated by the wide distribution of the posterior means) was p, showing that the probability of detection requires more data to estimate accurately than the other model parameters. In particular, p_r and p_d are estimated with very high accuracy and precision. The two domestic spread parameters ω_1 and ω_2 are estimated with higher precision than the importation rate γ, but with slightly less accuracy. We expect that the parameter estimate accuracy and precision would increase for all parameters with increasing sampling occasions T, sampling sites M, and simulation runs.

Listing S1: R code for data generating algorithm for simulation study.

```
impossible = TRUE
counter = 0

while (impossible) {
  counter = counter+1

  if (counter > 1000000) {
    stop("FAILED TO GENERATE")
  }

  Nit = matrix(0, nrow=2, ncol=30)
  Ait = matrix(0, nrow=2, ncol=29)
  Rit = matrix(0, nrow=2, ncol=29)
  Dit = matrix(0, nrow=2, ncol=30)
  Sit = matrix(0, nrow=2, ncol=29)
  Git = matrix(0, nrow=2, ncol=29)
  ait = matrix(0, nrow=2, ncol=30)
  nit = matrix(0, nrow=2, ncol=30)
  rit = matrix(0, nrow=2, ncol=30)

  Nit[,1] = rpois(2,true_lambda)
  nit[,1] = rbinom(2,Nit[,1], true_p_det)
```

```r
ait[,1] = nit[,1]

for (site in 1:2) {
  for (time in 2:30) {
    Dit[site,time-1] = rbinom(1,Nit[site,time-1], true_p_mor)

    Rit[site,time-1] = rbinom(1,Nit[site,time-1]-Dit[site,time-1],
            true_p_rec/(1-true_p_mor))

    Ait[site,time-1] = Nit[site,time-1]-Dit[site,time-1]-
            Rit[site,time-1]

    Sit[site,time-1] = rpois(1,true_omega1*(Nit[site, time-1]-
            ait[site, time-1]) + true_omega2*ait[site, time-1])

    Git[site,time-1] = rpois(1,true_gamma)

    Nit[site,time]   = Ait[site,time-1] + Sit[site,time-1] +
            Git[site,time-1]

    nit[site,time]   = rbinom(1,Nit[site,time]-ait[site,time-1],
            true_p_det)

    rit[site,time-1] = rbinom(1,ait[site,time-1]+nit[site,time]-
            Dit[site,time-1],true_p_rec/(1-true_p_mor/true_p_det))

    ait[site,time]   = ait[site,time-1]+nit[site,time]-
            Dit[site,time-1]-rit[site,time-1]
  }
}

if(!any(is.na(nit))) {
  impossible=FALSE
}
}
```

Figure S9 shows the running posterior means for each parameter for one run of the simulation (run 25 out of 50). The posterior means are each seen to converge close to the ground truth values rapidly, with only small changes after 1,000 iterations. The stability of the running posterior means shows good mixing and convergence of the posterior distributions. The other simulation runs had similar results.

For N-mixture type models, there has been substantial literature discussing lack of identifiability for p when the counts $\{n_{it}\}$ are small and when the number of sampling occasions T is small (Dennis et al., 2015; Barker et al., 2018). Our model may avoid this small p problem entirely due to the use of additional data through $\{r_{it}\}$ and $\{D_{it}\}$, as well as the additional model structure through the multinomial state process. However, should this work be applied to models fit with very small count sizes and very few sampling occasions, additional simulation studies may be required to verify parameter identifiability in that setting.

S.3 Average Recovery Times

Calculating average recovery time $\bar{p}_r$ using weekly probability of recovery (p_r) and weekly probability of remaining an active case (p_a) requires solving a simple geometric series in p_a. The geometric series arises from the repeated chance of recovery for each week of remaining active, and can be seen as the infinite sum: $S = p_r + p_r p_a + p_r p_a^2 + ... = p_r \sum_{k=0}^{\infty} p_a^k$. We can consider the partial sums $S_K = p_r \sum_{k=0}^{K} p_a^k$. Then, S_K is the total probability of recovery up to week K.

When $S_K = 0.5$, $K + 1$ is the number of weeks required for an average recovery. Note that it is $K + 1$ and not K due to the definition of p_r and p_a as probabilities between sampling occasions. The well known partial sum solution for the geometric series is: $S_K = p_r p_a^{K+1} / (p_a - 1)$. Rearranging to solve for K:

$$K = -1 + \log\left(\frac{S_K}{p_r}(p_a - 1) + 1\right) \bigg/ \log p_a.$$

Using our Canada wide estimates for the early pandemic time period ($\widehat{p}_r = 0.350$, and $\widehat{p}_a = 0.647$), we calculate $K + 1 = 1.61$. This means that the expected recovery time is, 161% of one week, or 11.3 days ($\bar{p}_r = 11.3$). Our reported 95% recovery interval of (6.1, 15.4) days for the early pandemic period was calculated using the exact same procedure but with $S_K = 0.025$ for the lower bound and $S_K = 0.975$ for the upper bound.

S.4 Supplementary Tables

Table S1: Average weekly probabilities of death in percent (%) for active COVID-19 cases (including unreported cases) split by three periods of the pandemic: Early Pandemic (prior to 4 Apr 2021), Delta (between 4 Apr and 28 Nov 2021), and Omicron (post 28 Nov 2021). 95% credible intervals are shown in parentheses.

Province/Territory	Early Pandemic	Delta	Omicron
Canada	0.257 (0.253,0.262)	0.164 (0.159,0.169)	0.063 (0.060,0.066)
Alberta	0.262 (0.258,0.266)	0.175 (0.171,0.180)	0.074 (0.071,0.076)
British Columbia	0.260 (0.256,0.264)	0.153 (0.148,0.157)	0.063 (0.061,0.066)
Manitoba	0.263 (0.259,0.267)	0.168 (0.164,0.173)	0.067 (0.064,0.069)
New Brunswick	0.262 (0.258,0.266)	0.155 (0.164,0.160)	0.056 (0.054,0.059)
Newfoundland and Labrador	0.261 (0.258,0.266)	0.136 (0.131,0.142)	0.041 (0.038,0.044)
Northwest Territories	0.238 (0.233,0.244)	0.187 (0.183,0.192)	0.078 (0.075,0.081)
Nova Scotia	0.264 (0.260,0.268)	0.152 (0.147,0.157)	0.054 (0.052,0.057)
Nunavut	0.251 (0.247,0.255)	0.198 (0.194,0.203)	0.068 (0.065,0.071)
Ontario	0.261 (0.257,0.265)	0.160 (0.155,0.164)	0.067 (0.064,0.069)
Prince Edward Island	0.262 (0.258,0.266)	0.151 (0.146,0.156)	0.056 (0.053,0.058)
Quebec	0.258 (0.254,0.263)	0.152 (0.147,0.157)	0.061 (0.059,0.064)
Saskatchewan	0.261 (0.257,0.265)	0.172 (0.168,0.176)	0.070 (0.067,0.072)
Yukon	0.241 (0.236,0.246)	0.172 (0.168,0.177)	0.064 (0.062,0.066)

Table S2: Average weekly probabilities of recovery in percent (%) for active COVID-19 cases split by three periods of the pandemic: Early Pandemic (prior to 4 Apr 2021), Delta (between 4 Apr and 28 Nov 2021), and Omicron (post 28 Nov 2021). 95% credible intervals are shown in parentheses.

| Province/Territory	Early Pandemic	Delta	Omicron
Canada	35.0 (34.9,35.0)	43.4 (43.3,43.5)	29.3 (29.2,29.4)
Alberta	34.5 (34.5,34.6)	42.5 (42.4,42.6)	28.4 (28.4,28.5)
British Columbia	34.7 (34.7,34.8)	45.0 (44.9,45.1)	29.0 (28.9,29.0)
Manitoba	34.4 (34.3,34.4)	43.0 (42.8,43.1)	28.9 (28.8,29.0)
New Brunswick	34.5 (34.5,34.6)	44.7 (44.6,44.8)	29.8 (29.7,29.9)
Newfoundland and Labrador	34.6 (34.5,34.7)	47.0 (46.9,47.2)	30.8 (30.8,30.9)
Northwest Territories	36.8 (36.7,36.9)	39.8 (39.7,39.9)	28.3 (28.2,28.4)
Nova Scotia	34.3 (34.2,34.3)	45.0 (44.9,45.1)	29.8 (29.7,29.9)
Nunavut	35.5 (35.4,35.5)	39.5 (39.4,39.6)	30.2 (30.2,30.3)
Ontario	34.6 (34.5,34.7)	44.1 (44.0,44.2)	28.7 (28.7,28.8)
Prince Edward Island	34.4 (34.4,34.5)	45.3 (45.2,45.4)	29.5 (29.5,29.6)
Quebec	35.0 (34.9,35.1)	45.0 (44.9,45.1)	29.2 (29.1,29.3)
Saskatchewan	34.7 (34.6,34.7)	43.0 (42.9,43.1)	28.9 (28.9,29.0)
Yukon	36.5 (36.4,36.6)	40.6 (40.5,40.7)	29.1 (29.1,29.2)

Table S3: Average weekly domestic spread rates for unobserved cases (ω_1) split by three periods of the pandemic: Early Pandemic (prior to 4 Apr 2021), Delta (between 4 Apr and 28 Nov 2021), and Omicron (post 28 Nov 2021). 95% credible intervals are shown in parentheses.

Province/Territory	Early Pandemic	Delta	Omicron
Canada	0.57 (0.55,0.59)	0.65 (0.63,0.67)	1.19 (1.17,1.21)
Alberta	0.61 (0.60,0.61)	0.71 (0.70,0.72)	1.25 (1.24,1.25)
British Columbia	0.54 (0.54,0.55)	0.57 (0.56,0.57)	1.16 (1.16,1.17)
Manitoba	0.61 (0.61,0.62)	0.69 (0.68,0.70)	1.23 (1.22,1.24)
New Brunswick	0.50 (0.49,0.52)	0.53 (0.52,0.55)	1.09 (1.07,1.10)
Newfoundland and Labrador	0.61 (0.59,0.63)	0.56 (0.54,0.58)	1.15 (1.13,1.17)
Northwest Territories	0.47 (0.44,0.51)	0.74 (0.70,0.77)	1.21 (1.18,1.25)
Nova Scotia	0.61 (0.59,0.62)	0.61 (0.60,0.63)	1.18 (1.16,1.19)
Nunavut	0.46 (0.44,0.49)	0.70 (0.68,0.73)	1.09 (1.07,1.12)
Ontario	0.59 (0.58,0.59)	0.63 (0.63,0.64)	1.21 (1.20,1.22)
Prince Edward Island	1.19 (1.11,1.26)	1.19 (1.12,1.26)	1.77 (1.70,1.84)
Quebec	0.37 (0.37,0.37)	0.40 (0.39,0.40)	0.99 (0.98,0.99)
Saskatchewan	0.52 (0.51,0.53)	0.62 (0.61,0.63)	1.15 (1.14,1.16)
Yukon	0.32 (0.25,0.36)	0.52 (0.44,0.56)	0.99 (0.91,1.04)

Table S4: Average weekly domestic spread rates for observed cases (ω_2) split by three periods of the pandemic: Early Pandemic (prior to 4 Apr 2021), Delta (between 4 Apr and 28 Nov 2021), and Omicron (post 28 Nov 2021). 95% credible intervals are shown in parentheses.

| Province/Territory	Early Pandemic	Delta	Omicron
Canada	0.17 (0.14,0.32)	1.45 (1.34,1.66)	1.37 (1.22,1.62)
Alberta	0.12 (0.12,0.13)	1.35 (1.27,1.44)	1.28 (1.15,1.42)
British Columbia	0.13 (0.12,0.14)	1.57 (1.48,1.67)	1.32 (1.18,1.47)
Manitoba	0.07 (0.07,0.07)	1.35 (1.26,1.45)	1.28 (1.15,1.43)
New Brunswick	0.09 (0.08,0.11)	1.52 (1.43,1.62)	1.38 (1.24,1.53)
Newfoundland and Labrador	0.09 (0.09,0.10)	1.74 (1.65,1.84)	1.49 (1.33,1.65)
Northwest Territories	0.41 (0.30,0.73)	1.19 (1.02,1.51)	1.34 (1.16,1.66)
Nova Scotia	0.06 (0.05,0.06)	1.55 (1.46,1.64)	1.38 (1.23,1.53)
Nunavut	0.19 (0.17,0.26)	1.05 (0.95,1.15)	1.41 (1.30,1.54)
Ontario	0.09 (0.09,0.09)	1.46 (1.37,1.55)	1.27 (1.13,1.42)
Prince Edward Island	0.13 (0.08,0.37)	1.64 (1.52,1.90)	1.42 (1.25,1.71)
Quebec	0.22 (0.22,0.23)	1.64 (1.55,1.74)	1.41 (1.27,1.56)
Saskatchewan	0.18 (0.16,0.19)	1.43 (1.35,1.52)	1.37 (1.24,1.50)
Yukon	0.43 (0.28,1.63)	1.31 (1.11,2.51)	1.47 (1.25,2.67)

Table S5: Results from fitting our multi-site model with various covariate structures. All models used site as a covariate for λ. All models considered no covariates for p_d and p_r. Each parameter column indicates which covariates were considered for the given parameter. Phase of B.C. Recovery Plan is indicated by pha. Health Authority Region is indicated by reg. Virus testing volume is indicated by vol. A baseline offset which is the same for each region is indicated by B. Models for which $\omega_1 = \omega_2$ are indicated as such in the ω_2 column (if $\omega_1 = \omega_2$ is not indicated here, ω_1 and ω_2 are not forced to be equal). Column **Q** shows the number of trained parameters in each model. Column **WAIC** shows the WAIC for each model, while Δ**WAIC** shows the difference in WAIC compared with the best performing model.

| Model	γ	ω_1	ω_2	p	Q	WAIC	ΔWAIC
M1	(*pha*, *reg*)	(*pha*, *reg*)	(*pha*, *reg*)	(*pha*, *reg*)	43	5674	0
M2	(*pha*, *reg*)	(*pha*)	(*pha*)	(*vol*)	25	6223	549
M3	(*pha*, *reg*)	(*pha*, *reg*)	(*pha*, *reg*)	(*vol*)	35	6234	560
M4	(*pha*, *reg*)	(*pha*, *reg*)	(*pha*, *reg*)	(*pha*, *vol*)	39	6257	583
M5	(*pha*, *reg*)	(*pha*)	(*pha*)	(*pha*, *reg*)	33	6316	642
M6	(*pha*, *reg*)	(*pha*)	(*pha*)	(*B*, *vol*)	26	6332	658
M7	(*pha*, *reg*)	(*pha*, *reg*)	(*pha*, *reg*)	(*pha*, *reg*, *vol*)	44	6337	663
M8	(*pha*, *reg*)	(*pha*, *reg*)	(*pha*, *reg*)	(*reg*, *vol*)	40	6442	768
M9	(*pha*, *reg*)	(*pha*)	(*pha*)	(*reg*, *vol*)	30	6454	780
M10	(*pha*, *reg*)	(*pha*, *reg*)	(*pha*, *reg*)	(*B*, *vol*)	36	6517	843
M11	(*pha*, *reg*)	(*pha*, *reg*)	$\omega_1 = \omega_2$	(*pha*, *reg*, *vol*)	35	6541	867
M12	(*pha*, *reg*)	(*pha*)	$\omega_1 = \omega_2$	(*vol*)	21	6625	951
M13	(*pha*, *reg*)	(*pha*, *reg*)	$\omega_1 = \omega_2$	(*pha*, *vol*)	30	6658	984
M14	(*pha*, *reg*)	(*pha*)	$\omega_1 = \omega_2$	(*pha*, *reg*)	29	6695	1021
M15	(*pha*, *reg*)	(*pha*)	$\omega_1 = \omega_2$	(*pha*, *reg*, *vol*)	30	6702	1028
M16	(*pha*, *reg*)	(*pha*)	$\omega_1 = \omega_2$	(*pha*, *vol*)	25	6773	1099
M17	(*pha*, *reg*)	(*pha*)	$\omega_1 = \omega_2$	(*reg*, *vol*)	26	6798	1124
M18	(*pha*, *reg*)	(*pha*)	$\omega_1 = \omega_2$	(*B*, *vol*)	22	6868	1194
M19	(*reg*)	(none)	(none)	(*reg*, *vol*)	20	7039	1365
M20	(*reg*)	(none)	(none)	(*B*, *vol*)	16	7058	1384
M21	(*reg*)	(none)	(none)	(*pha*, *reg*)	23	7131	1384
M22	(*reg*)	(none)	(none)	(*pha*, *reg*, *vol*)	24	7304	1630

S.5   Supplementary Figures
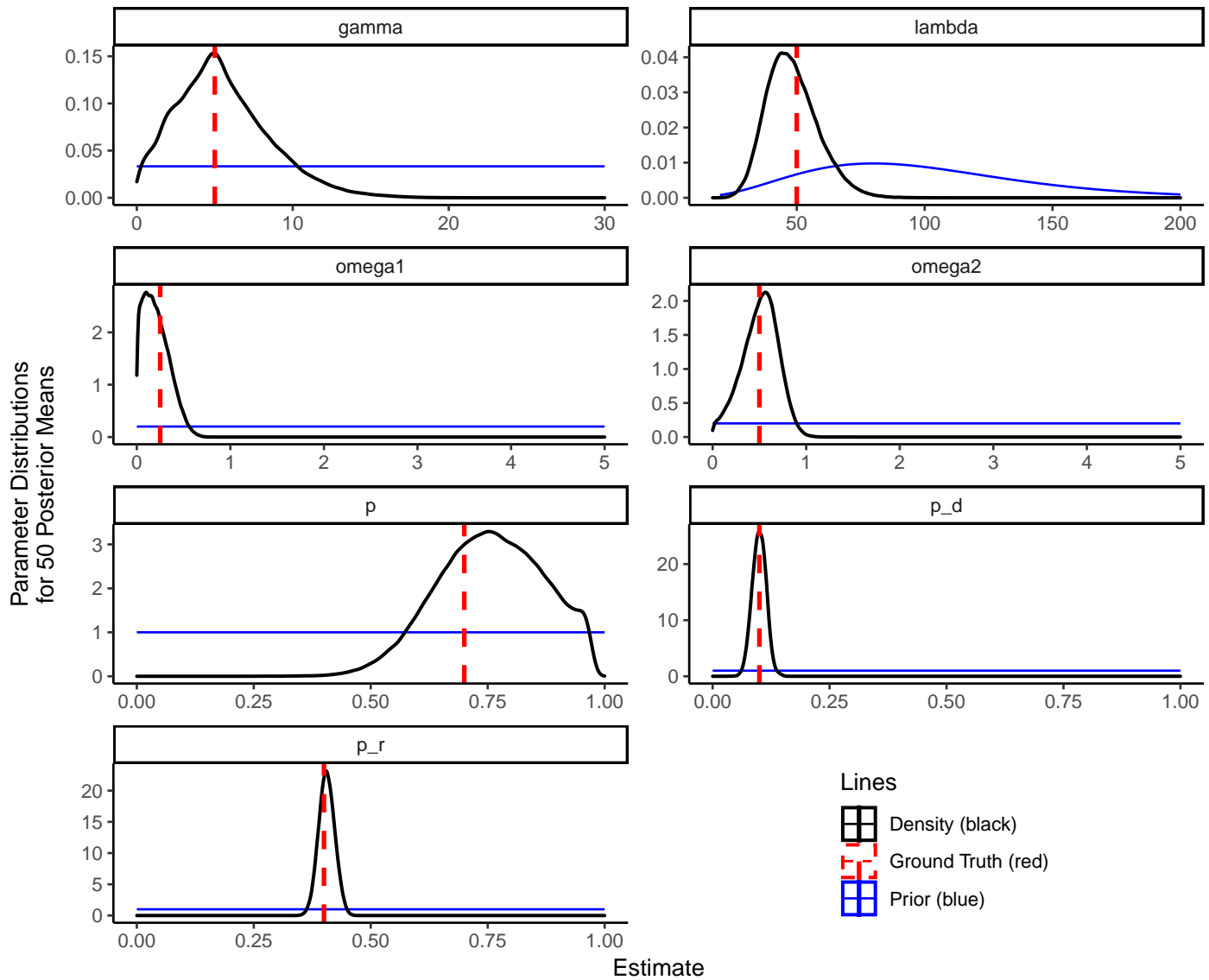
Figure S8: Density plots showing posterior means for each estimated parameter. Fifty simulation runs were used. Red dashed lines indicate the ground truth parameter values for the simulation. Posterior modes are close to ground truth parameter values.
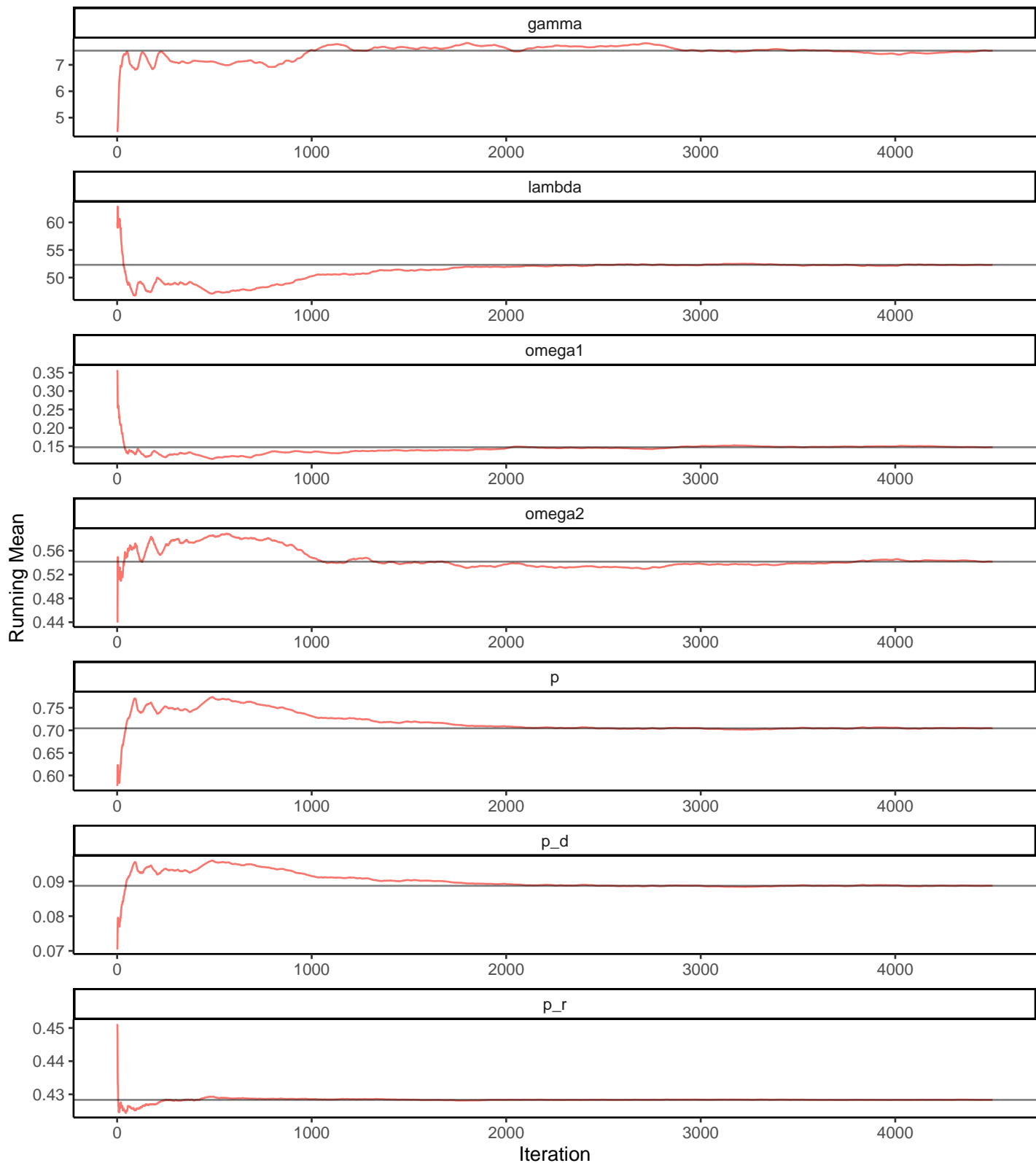
Figure S9: Posterior running means for each estimated parameter for a single fixed replicate (dataset 25 out of 50) of the simulation study. The black horizontal lines indicate the overall mean. Red lines indicate the running means. Running means approach overall means.
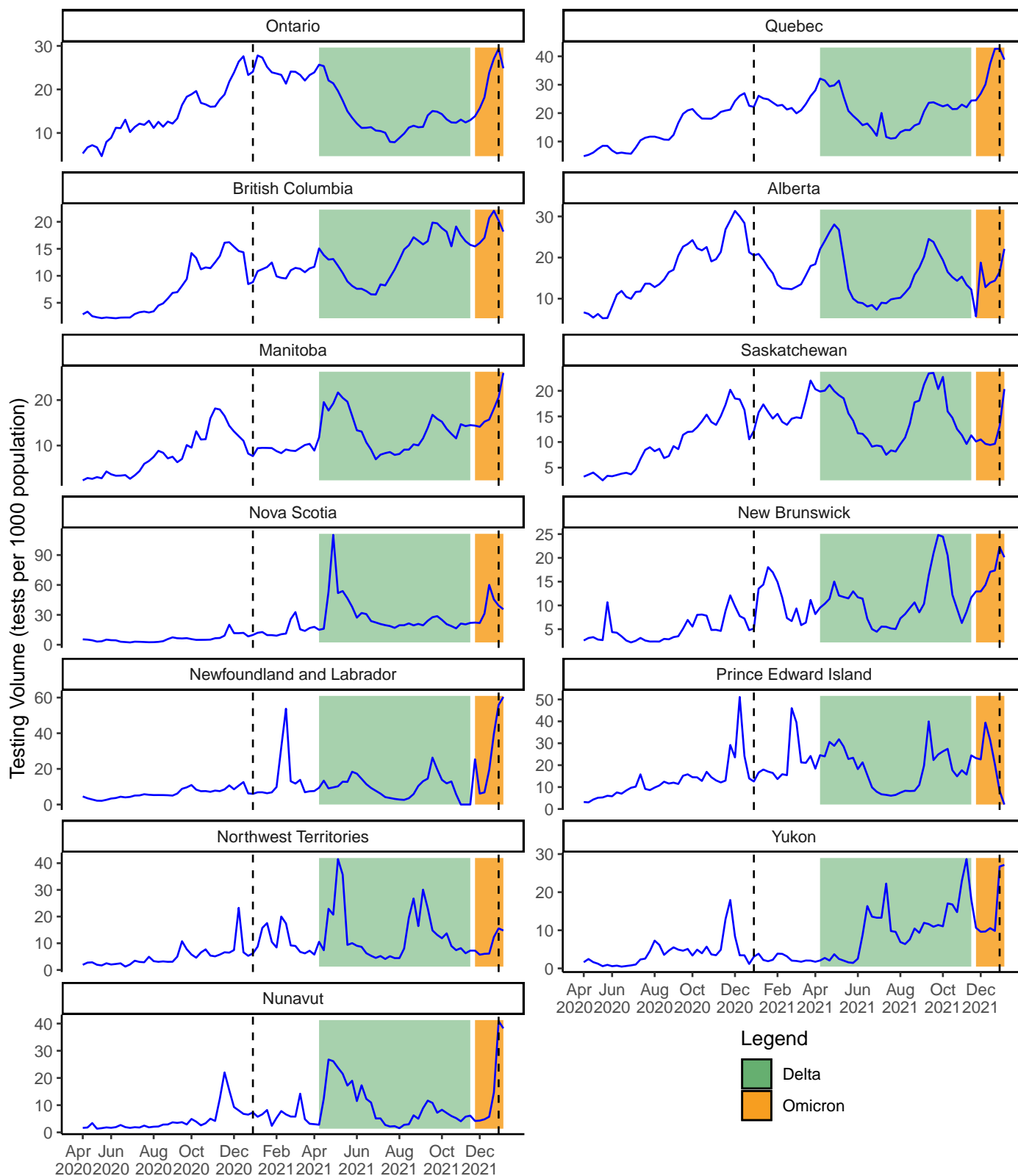
Figure S10: Testing volumes per 1,000 population for each province/territory from 2 Apr 2020 to 6 Jan 2022. The time periods for the two variants of concern Delta and Omicron are depicted with coloured bands, indicating the first observations in Canada. The two vertical dashed lines indicate 1 Jan 2021 and 1 Jan 2022.
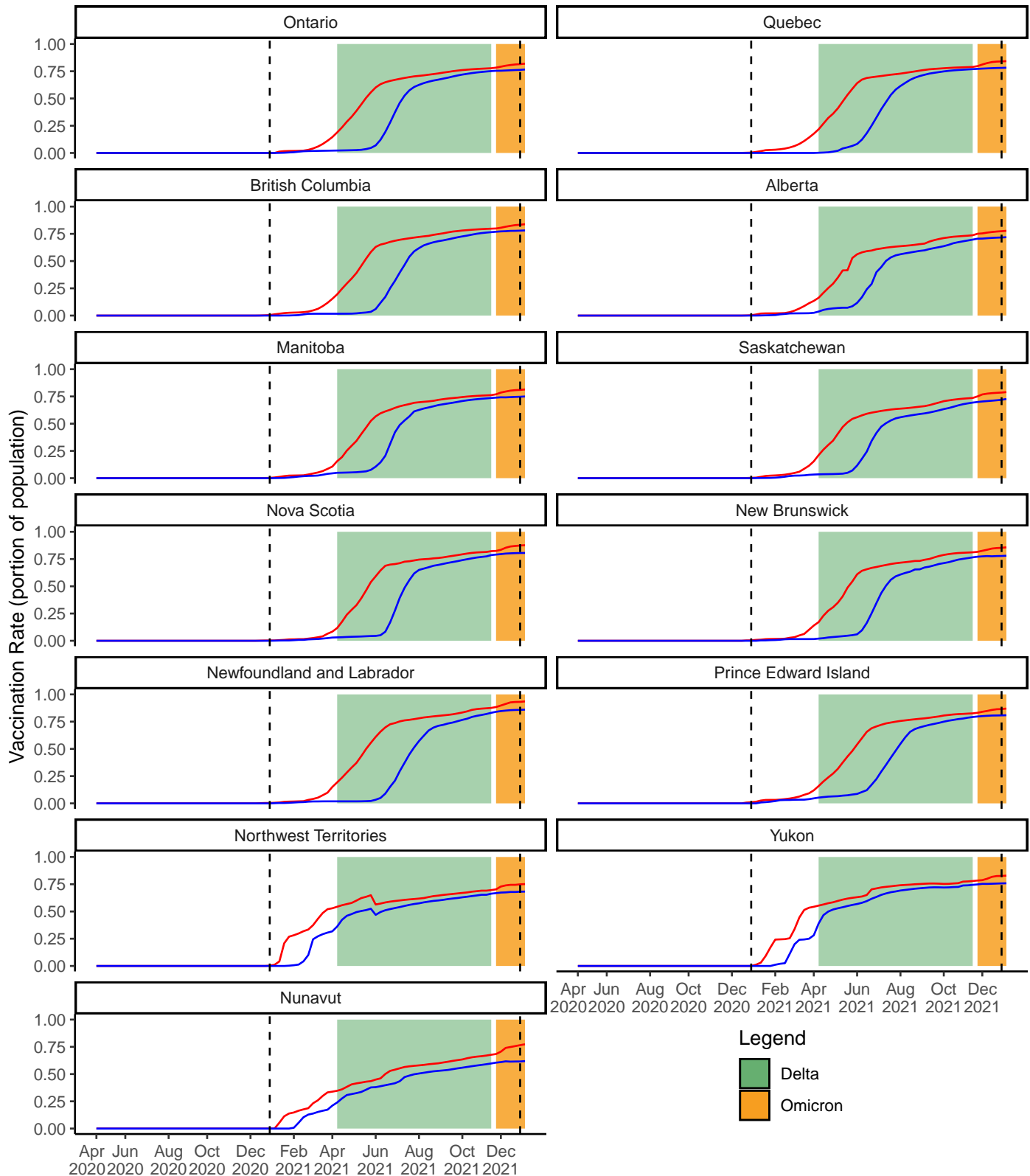
Figure S11: Vaccination rate for each province/territory from 2 Apr 2020 to 6 Jan 2022. The red line indicates at least 1 vaccination dose. The blue line indicates 2 doses. A vaccination rate of 0.5 indicates 50% of the population is vaccinated. The time periods for the two variants of concern Delta and Omicron are depicted with coloured bands, indicating the first observations in Canada. The two vertical dashed lines indicate 1 Jan 2021 and 1 Jan 2022.
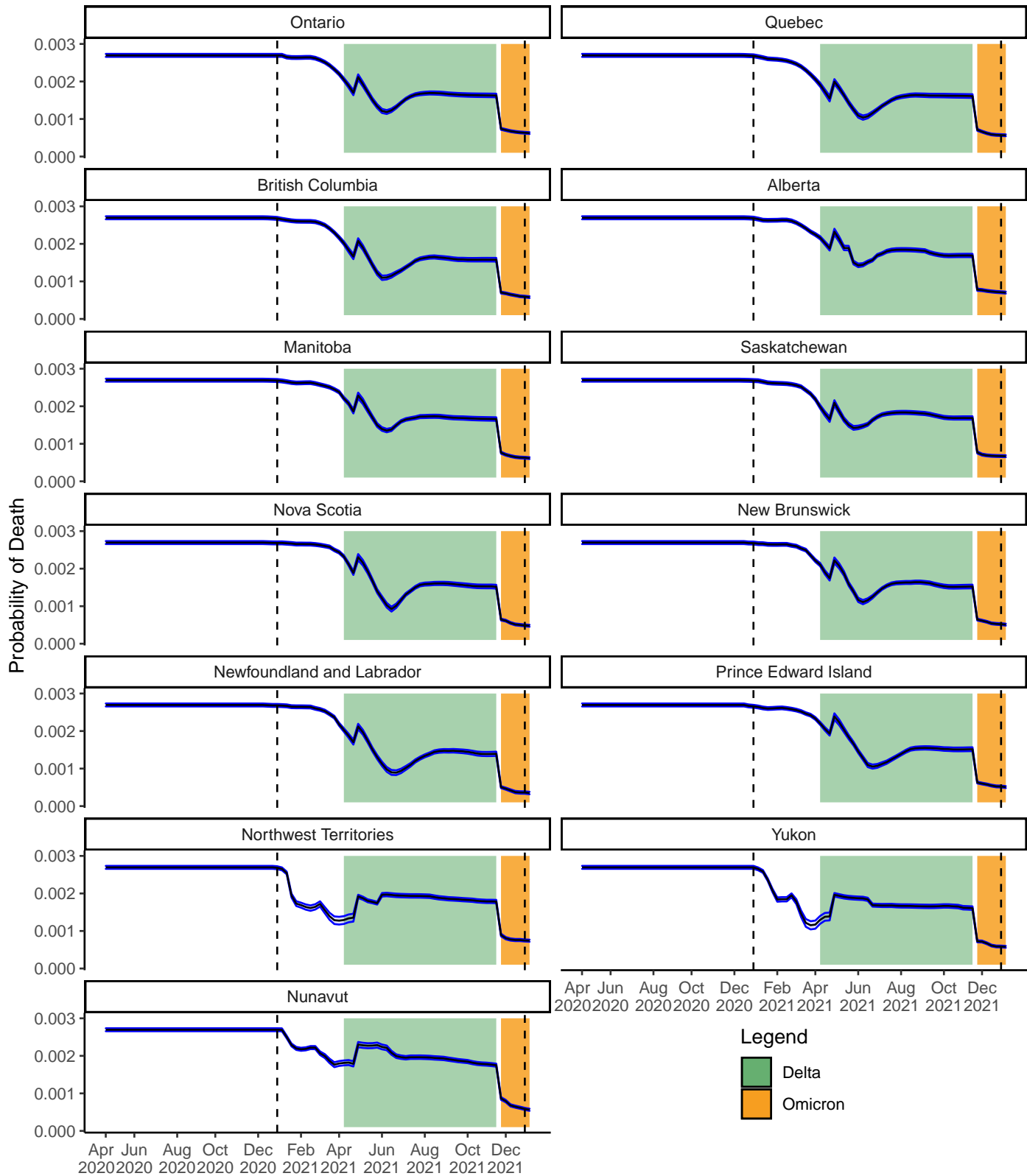
Figure S12: Estimated weekly probability of death (blue) for active COVID-19 cases for each province/territory from 2 Apr 2020 to 6 Jan 2022. The time periods for the two variants of concern Delta and Omicron are depicted with coloured bands, indicating the first observations in Canada. The two vertical dashed lines indicate 1 Jan 2021 and 1 Jan 2022. Bands show 95% credible intervals.
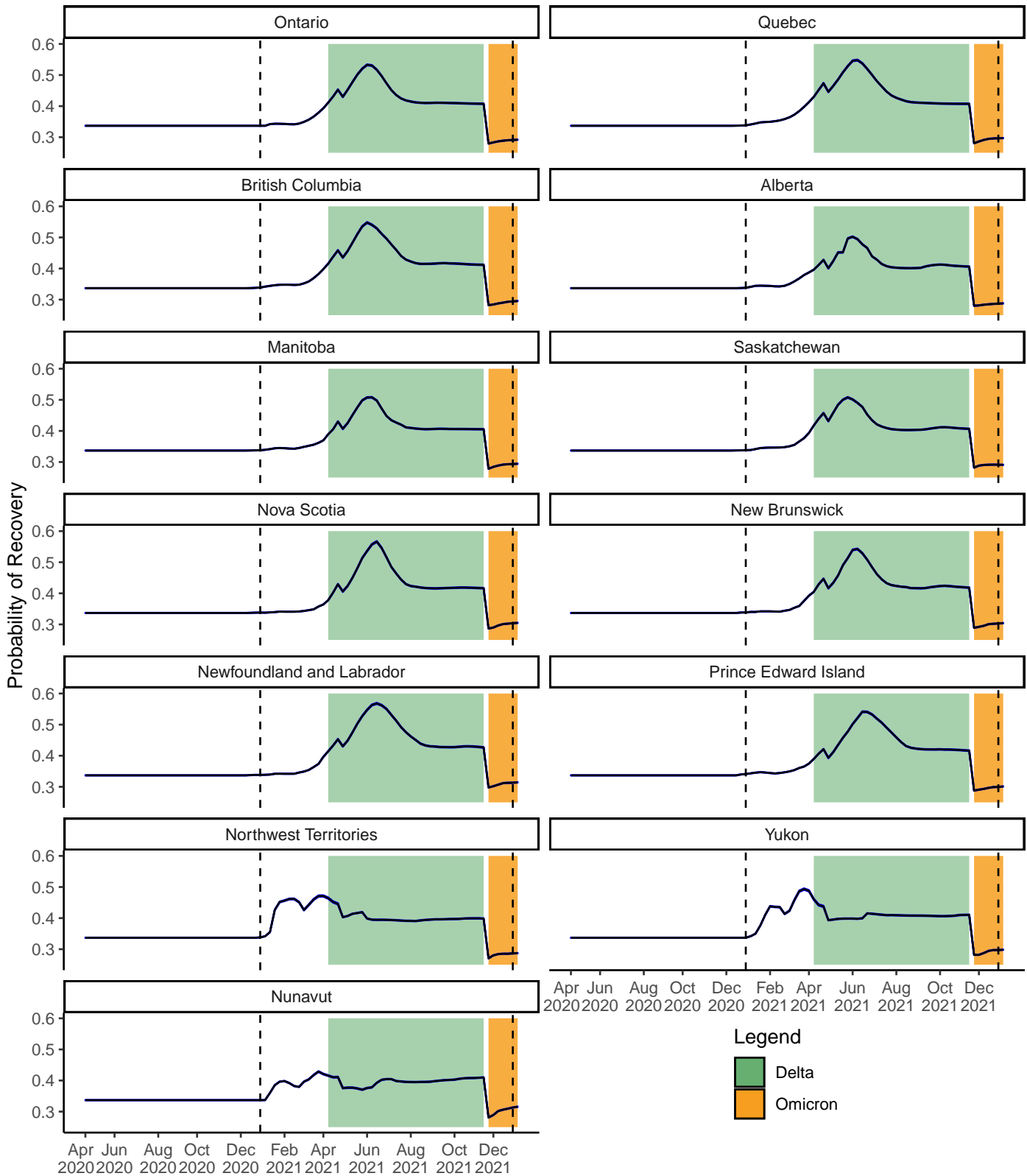
Figure S13: Estimated weekly probability of recovery (blue) for active COVID-19 cases for each province/territory from 2 Apr 2020 to 6 Jan 2022. The time periods for the two variants of concern Delta and Omicron are depicted with coloured bands, indicating the first observations in Canada. The two vertical dashed lines indicate 1 Jan 2021 and 1 Jan 2022. Bands show 95% credible intervals.
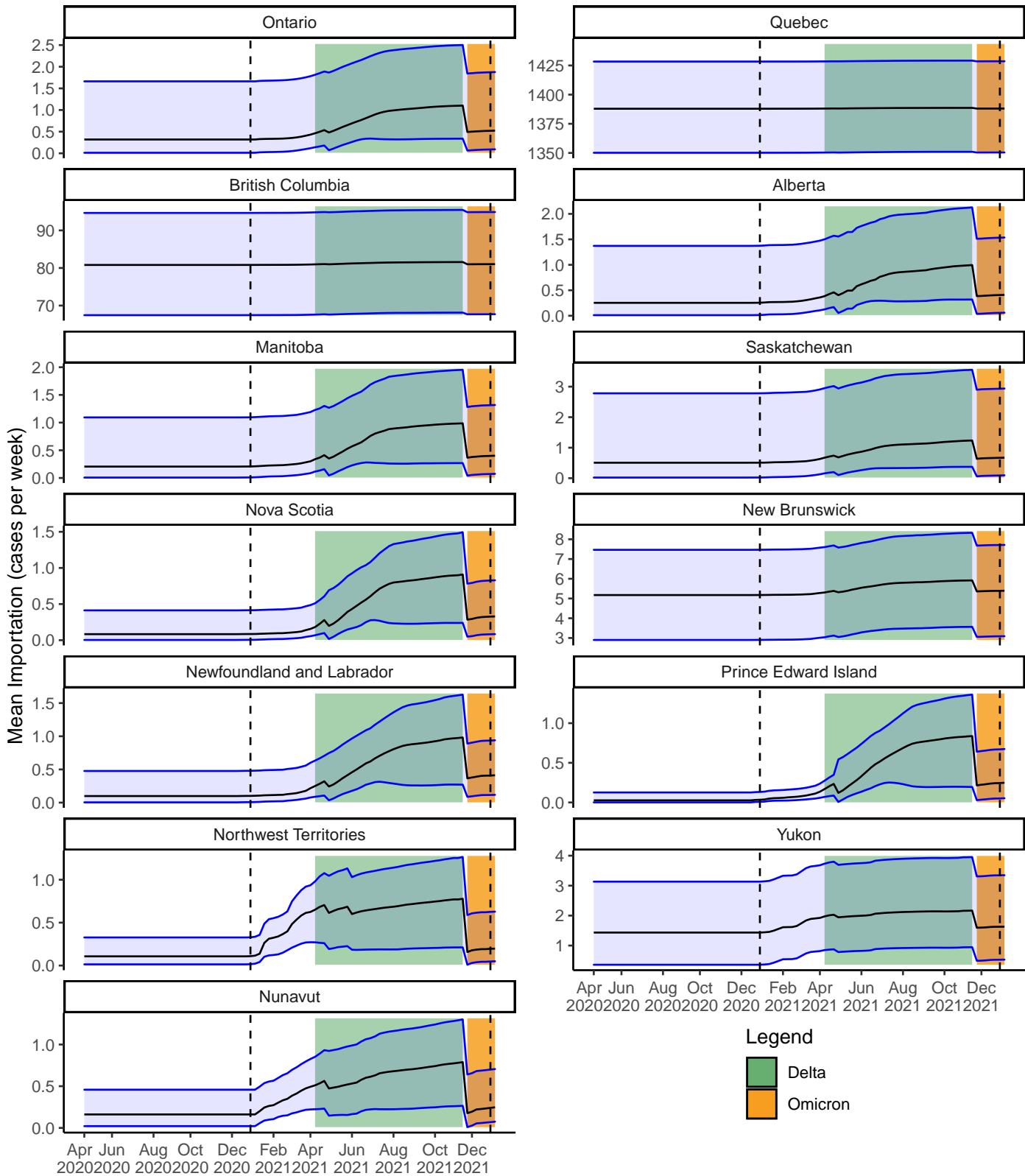
Figure S14: Estimated weekly importation of active COVID-19 cases for each province/territory from 2 Apr 2020 to 6 Jan 2022. The time periods for the two variants of concern Delta and Omicron are depicted with coloured bands, indicating the first observations in Canada. The two vertical dashed lines indicate 1 Jan 2021 and 1 Jan 2022. Bands show 95% credible intervals.
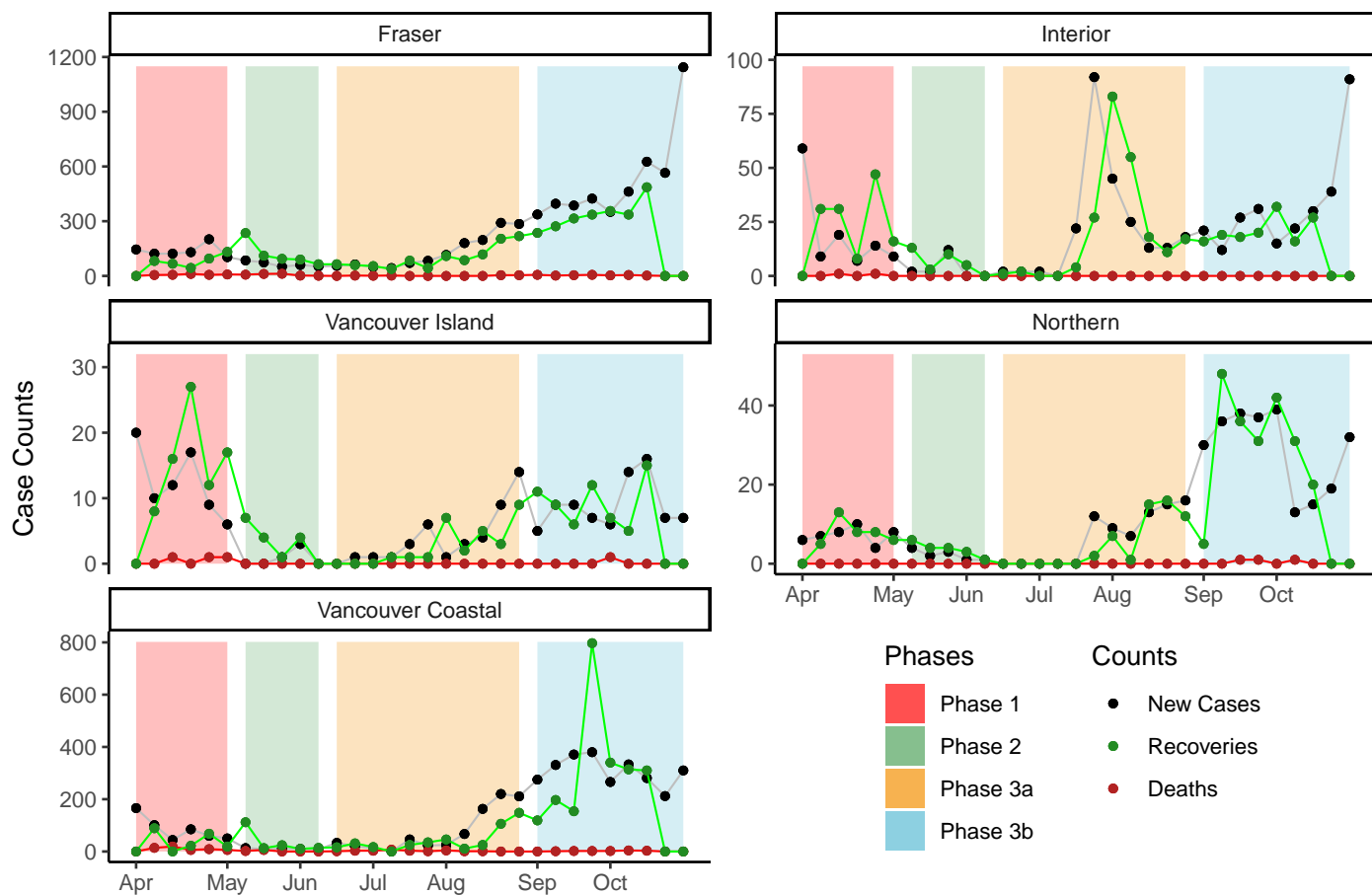
Figure S15: Plots of observed active cases (black), recoveries (green) and deaths (red) in B.C., split by Health Authority Region. Data starts on 2 Apr 2020 (Week 1) and ends on 30 Oct 2020 (Week 31).
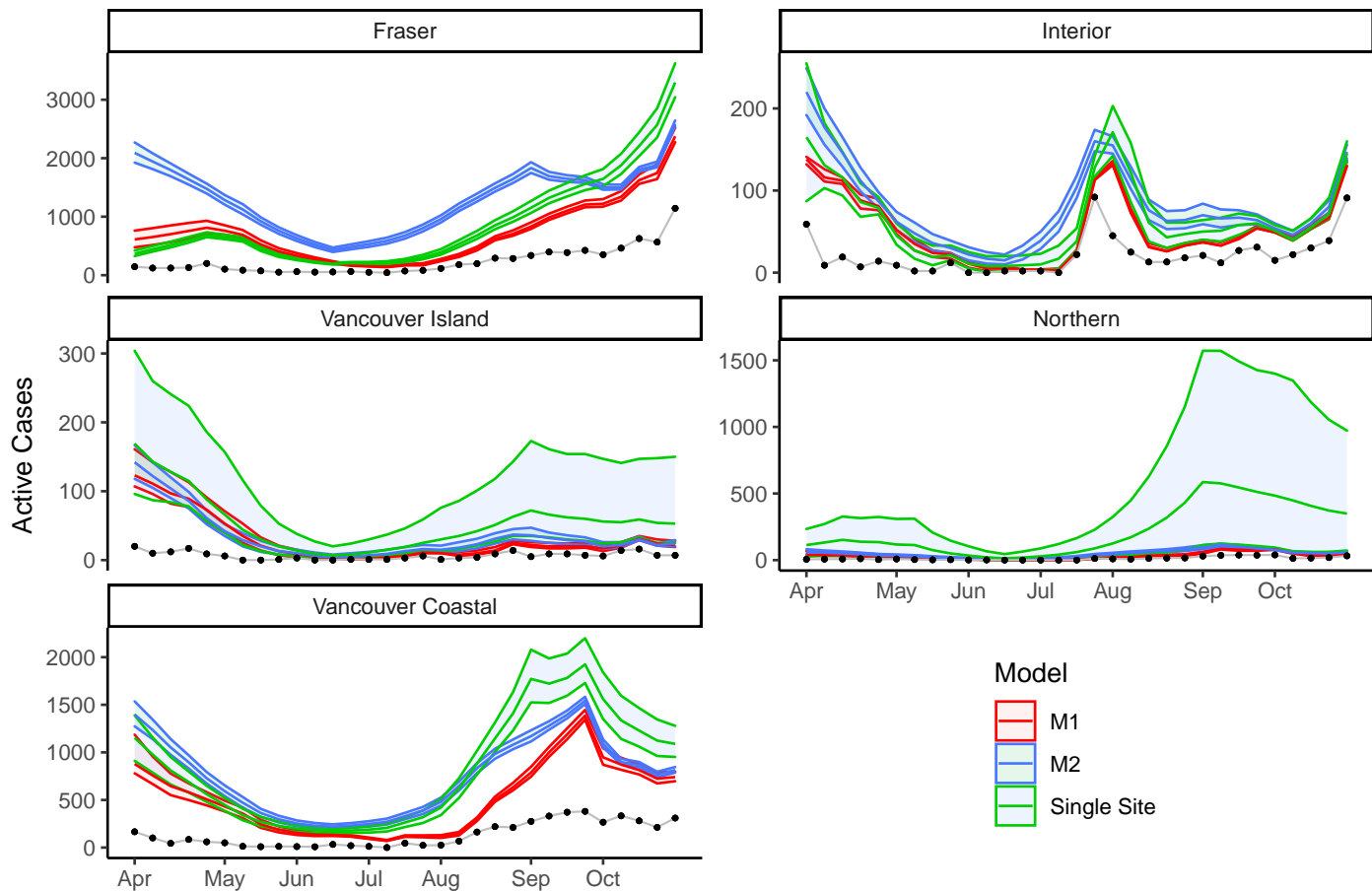
Figure S16: Plots of active cases split by Health Authority Region of B.C. Data starts on 2 Apr 2020 (Week 1) and ends on 30 Oct 2020 (Week 31). The red bands show the 95% credible intervals for total active cases as estimated using model M1, the best fitted model according to WAIC. The blue bands show the 95% credible intervals for total active cases as estimated using model M2, the second best fitted model according to WAIC. The green bands show the 95% credible intervals for total active cases as estimated using the single site models with testing volume as a covariate for detection probability. The black dotted line shows the newly observed active cases each week (according to data).
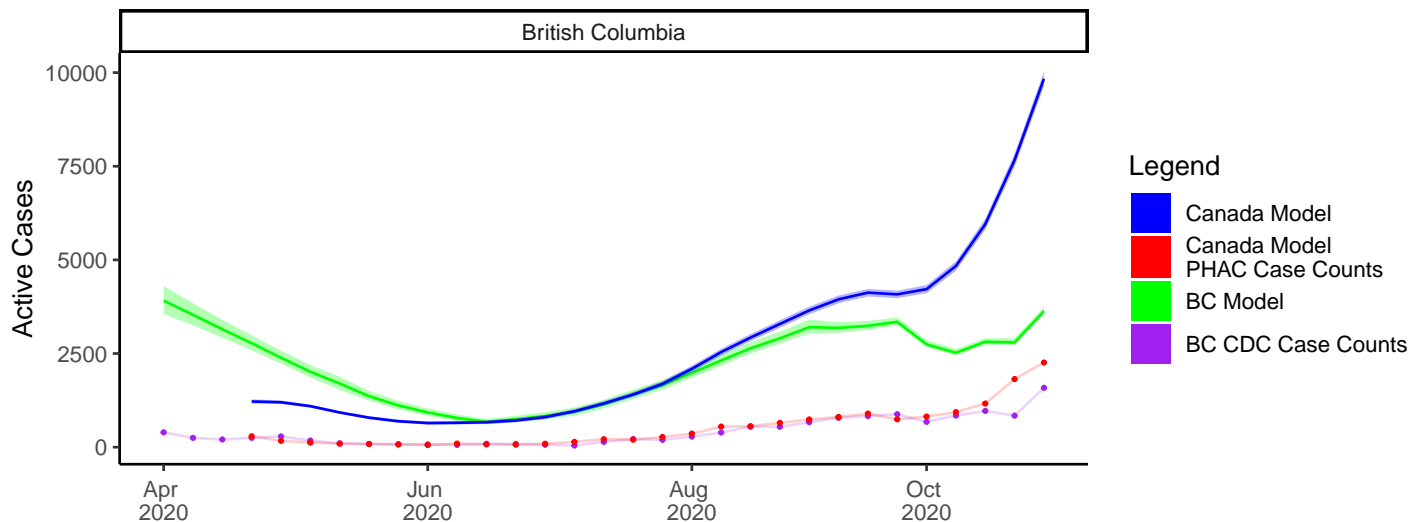
Figure S17: Plots of total active cases for B.C. Data starts on 2 Apr 2020 (Week 1) and ends on 30 Oct 2020 (Week 31). Note that the Canada model data starts on date 23 Apr 2020 (Week 4 of the B.C. only model). The blue bands show the 95% credible intervals for total active cases. Results from the B.C. Health Authority case study, summed over regions, are shown in green, with data shown in purple. Results from the Canada case study, subset to B.C. and Weeks 1 to 31, are shown in blue, with data shown in red. The black dotted line shows the newly observed active cases each week.

S.6   Supplementary Code

Data and code for the B.C. and Canada-wide case studies are available at `https://github.com/mrpar`
`ker909/COVID-MultiSiteModel2022.git`.